Crustal structure beneath the Galápagos Archipelago from ambient noise tomography and its implications for plume-lithosphere interactions

Darwin R. Villagómez,[1] Douglas R. Toomey,[1] Emilie E. E. Hooft,[1] and Sean C. Solomon[2]

Received 9 June 2010; revised 20 December 2010; accepted 10 January 2011; published 19 April 2011.

[1] To constrain the seismic velocity structure of the crust beneath the Galápagos Archipelago, we conducted a tomographic study using high-frequency Rayleigh waves obtained from cross correlations of ambient noise. We analyzed waves with periods between 5 and 8.5 s, sensitive to shear wave velocity (V_S) structure between about 3 and 10 km depth, after accounting for the effect of water depth. Crustal velocities are up to 25% lower than those of very young crust at the East Pacific Rise and are comparable to those of Hawaii. We attribute the lower than normal velocities to the combined effect of heating and the presence of melt in the crust above the Galápagos plume as well as the construction of a highly porous volcanic platform emplaced atop preexisting oceanic crust. On average, V_S between 3 and 10 km depth beneath the western archipelago is up to 15% lower than beneath the eastern archipelago. We attribute the west-to-east velocity increase to a decrease in porosity of the volcanic platform and to cooling of the crust after its passage above the Galápagos plume. The results of this study, in combination with previous work, indicate that many of the unusual aspects of the Galápagos Archipelago are the result of variations in the thickness and internal structure of the chemical and thermal lithospheres. Our findings indicate that observed variations in the flexural response to loading observed in the Galápagos cannot be explained by the current thermal state of the lithosphere. Instead, the flexural response likely represents varying elastic strength at the time of loading. We also propose that the northwest and northeast trending alignments of volcanic centers found throughout the archipelago (the Darwinian lineations) may be associated with preexisting zones of weakness in the lithosphere formed during earlier episodes of ridge jumping and ridge propagation that were later reactivated by stresses generated by plume-lithosphere interactions.

Citation: Villagómez, D. R., D. R. Toomey, E. E. E. Hooft, and S. C. Solomon (2011), Crustal structure beneath the Galápagos Archipelago from ambient noise tomography and its implications for plume-lithosphere interactions, *J. Geophys. Res.*, *116*, B04310, doi:10.1029/2010JB007764.

1. Introduction

[2] The Galápagos hot spot, located in the eastern equatorial Pacific (Figure 1), shares many of the characteristics of intraplate volcanic hot spots: (1) it is long lived, with age estimates from 20 to 22 Ma [*Hey*, 1977; *Lonsdale and Klitgord*, 1978] to 90 Ma [*Hauff et al.*, 1997]; (2) the composition and isotope ratios of the most recent lavas resemble those of other ocean island basalts [*Geist et al.*, 1988; *White et al.*, 1993]; (3) two volcanic chains or hot spot trails, the Cocos and Carnegie ridges, extend from the Galápagos in the directions of motion of the Cocos and Nazca plates; and (4) the seamounts of the Galápagos platform, and the Carnegie and Cocos ridges, generally increase in age with distance from the western edge of the archipelago [*Sinton et al.*, 1996; *Werner et al.*, 1999; *Hoernle et al.*, 2002]. Moreover, seismic studies have resolved anomalously low seismic velocities indicative of higher than normal temperatures in the upper mantle beneath the western archipelago [*Toomey et al.*, 2002; *Hooft et al.*, 2003; *Villagómez et al.*, 2007]. The plume hypothesis [*Morgan*, 1972] successfully explains these observations.

[3] However, two characteristics of the Galápagos Archipelago suggest that the hot spot differs from otherwise similar features. First, the Galápagos hot spot includes a spatially broad distribution of active volcanic centers [*McBirney and Williams*, 1969]. Nine volcanoes have been active historically, and an additional four have erupted in the Holocene [*White et al.*, 1993]. In contrast, there are only four active

[1]Department of Geological Sciences, University of Oregon, Eugene, Oregon, USA.
[2]Department of Terrestrial Magnetism, Carnegie Institution of Washington, Washington, D. C., USA.

0148-0227/11/2010JB007764

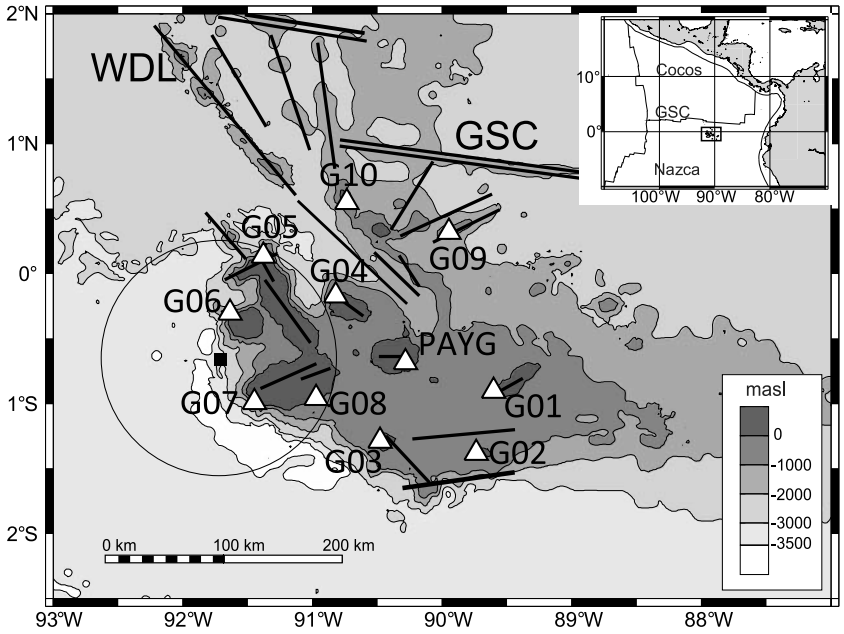

Figure 1. Map of the Galápagos Islands and seismic network. Triangles indicate seismic stations. Black square and solid circle with a 100 km radius indicate the approximate center and area of a region of anomalously thin mantle transition zone [*Hooft et al.*, 2003]. Thick black lines show lineations and volcanic alignments from *McBirney and Williams* [1969], *Feighner and Richards* [1994], and *Sinton et al.* [2003]. WDL is the Wolf-Darwin lineament, and GSC denotes the Galápagos Spreading Center. Topography and bathymetry (in meters above sea level, or masl) are from W. Chadwick (http://newport.pmel.noaa.gov/~chadwick/galapagos.html).

volcanoes associated with the Hawaiian hot spot, and only one at the Reunion hot spot. Second, recent Galápagos lavas show a considerable range in composition. Lavas from the central and eastern parts of the archipelago tend to have more depleted trace element and isotopic signatures, whereas lavas erupted from the western and southern periphery have more enriched signatures [*Geist et al.*, 1988; *White et al.*, 1993]. This pattern correlates with volcano morphology. The western volcanoes are young, large, central shield volcanoes with well-developed calderas, whereas the eastern volcanoes are generally older and smaller [*White et al.*, 1993]. Another distinctive characteristic of the Galápagos is that some volcanic centers and seamounts are aligned mostly along northeast and northwest trending lineations [*Darwin*, 1860; *McBirney and Williams*, 1969] (Figure 1).

[4] To investigate the nature of the Galápagos hot spot and archipelago, we conducted a broadband seismic experiment. Here we use high-frequency Rayleigh waves to image the regional seismic structure of the crust. Our results show anomalously low seismic velocities beneath the western archipelago between about 3 and 10 km depth. The low velocities and the velocity-depth gradient are consistent with increased porosity and temperature in the crust beneath the western archipelago. We also integrate these findings with results from earlier surface wave tomography [*Villagómez et al.*, 2007], plate reconstructions [*Wilson and Hey*, 1995; *Barckhausen et al.*, 2001; *Meschede and Barckhausen*, 2000], and gravity anomalies [*Sandwell and Smith*, 1997]. On the basis of this synthesis, we infer that many of the anomalous aspects of the Galápagos largely reflect the thickness and mechanical properties of the lithosphere that overlies the Galápagos plume.

2. Data and Methods

[5] Broadband seismic stations were deployed on nine islands of the archipelago between September 1999 and March 2003 (Figure 1). The network consisted of 10 portable broadband stations and the Global Seismographic Network station PAYG. The station spacing was between 50 and 70 km. Three-component Streckeisen STS-2 sensors were used at all portable stations; two Guralp CMG-3ESP instruments were initially deployed but were replaced after the first year. Data loggers were Reftek units recording continuously at 20 samples/s. The seismic network spanned an area approximately 200 km in diameter.

[6] For this study we extracted continuous vertical component records of seismic noise for 24 time periods from 11 to 50 days in duration between October 1999 and June 2002. We obtained estimates of the Rayleigh wave group velocity between periods of 5 and 8.5 s from cross correlations of pairs of noise records, from which we have inferred the shear wave velocity structure and present thermal state of the crust.

2.1. Imaging of Rayleigh Wave Group Velocity

[7] We have used the ambient noise tomographic method to infer aspects of the seismic velocity structure beneath the archipelago. The cross correlation of ambient noise at pairs of stations yields estimates of the interstation Green's function, which for station spacing between 30 and 500 km

is dominated by Rayleigh waves [e.g., *Shapiro and Campillo*, 2004; *Sabra et al.*, 2005; *Shapiro et al.*, 2005]. The cross-correlation technique is most effective when the noise amplitude is approximately uniform in space and time [*Shapiro and Campillo*, 2004; *Sabra et al.*, 2005], so the effects of large seismic events should be minimized before calculating the cross correlation. Several approaches can be taken to reduce the contribution of the most energetic arrivals, such as one bit, running absolute mean, or water level normalizations [*Bensen et al.*, 2007]. For this study we disregard the amplitude by keeping only the sign of the signals and correlating one-bit records [*Larose et al.*, 2004; *Malcolm et al.*, 2004; *Bensen et al.*, 2007]. This simple approach produces results with signal-to-noise ratios comparable to other methods [*Bensen et al.*, 2007], particularly in areas with low levels of regional seismicity such as the Galápagos.

[8] We measured the group velocity of Rayleigh waves derived from the station pair cross correlations using multiple filter analysis (MFA) (http://www.eas.slu.edu/People/RBHerrmann/CPS330.html). MFA provides a graphical assessment of the group velocities over a range of periods, thus allowing a user to determine an appropriate dispersion curve. Each cross correlation is filtered in a series of narrow pass bands with a Gaussian filter of the form [*Dziewonski et al.*, 1969]

$$H_n(\omega) = \exp\left[-\alpha\left(\frac{\omega-\omega_n}{\omega_n}\right)^2\right], \tag{1}$$

where ω is angular frequency, ω_n is the center frequency of the filter, and α is a parameter that controls the width of the filter in the frequency domain. The group arrival time corresponds to the peak in the envelope of the filtered signal. The envelopes are contoured as functions of period and group velocity to aid in the identification of the dispersion curve. The success of the MFA method depends on the correct identification of the fundamental mode dispersion curve and the appropriate truncation of measurements at short and long periods as the signal weakens (http://www.eas.slu.edu/People/RBHerrmann/CPS330.html).

[9] We used the group velocity measurements between pairs of stations to estimate both a regional average and lateral variations in group velocity. The propagation path is approximated by the geometric ray that connects the pair of stations. We consider this a good approximation to a more general approach that uses two-dimensional sensitivity kernels [*Ritzwoller et al.*, 2002; *Zhou et al.*, 2004], because we expect that at short periods and at regional scales both methods will recover similar structure [e.g., *Ritzwoller et al.*, 2002].

[10] To obtain lateral variations in group velocity (U), we parameterized the region as a series of blocks. The velocity $U_{\mathrm{L}}^{\mathrm{j}}$ estimated along the jth path between a pair of stations, L, can be expressed as

$$U_{\mathrm{L}}^{\mathrm{j}} = \sum_{i=1}^{m} f_{\mathrm{i}}^{\mathrm{j}} U_{\mathrm{i}}, \tag{2}$$

where $f_{\mathrm{i}}^{\mathrm{j}}$ corresponds to the fraction of the jth path that lies inside the ith block, U_{i} is the velocity inside the ith block, m is the total number of blocks or model parameters, and $\sum_{i=1}^{m} f_{\mathrm{i}}^{\mathrm{j}} = 1$.

[11] In matrix form, equation (2) becomes

$$\mathbf{U}_{\mathrm{L(n\times 1)}} = \mathbf{F}_{\mathrm{(n\times m)}}\mathbf{U}_{\mathrm{m\times 1}}, \tag{3}$$

where n is the total number of paths or observations, and the size of each matrix or vector is shown in parentheses. This is a linear system of equations, with a damped least squares solution [e.g., *Tikhonov*, 1943]

$$\mathbf{U} = \left(\mathbf{F}^{\mathrm{T}}\mathbf{C}_{\mathrm{d}}^{-1}\mathbf{F} + \beta^2\mathbf{I}\right)^{-1}\mathbf{F}^{\mathrm{T}}\mathbf{C}_{\mathrm{d}}^{-1}\mathbf{U}_{\mathrm{L}}, \tag{4}$$

where β is a weighting factor found by trial and error, and $\mathbf{I}$ is the identity matrix. $\mathbf{C_d}$ is the data covariance matrix, which, for uncorrelated velocity estimates, is equal to

$$(\mathbf{C}_{\mathrm{d}})_{\mathrm{ij}} = \delta_{\mathrm{ij}}\sigma_{\mathrm{i}}^2, \tag{5}$$

where σ_{i} is the uncertainty in the determination of $U_{\mathrm{L}}^{\mathrm{i}}$ and δ_{ij} is the Kronecker delta ($\delta_{\mathrm{ij}} = 0$ for $\mathrm{i} \neq \mathrm{j}$, $\delta_{\mathrm{ij}} = 1$ for $\mathrm{i} = \mathrm{j}$).

[12] For $\beta = 0$, equation (4) reduces to a least squares solution that depends only on the data. However, the least squares approach to the linear problem does not guarantee positivity of the solution. To ensure positivity, we can sacrifice linearity by parameterizing the model in terms of $r = \ln(U)$ and finding a solution using an iterative method [e.g., *Wilcock et al.*, 1995]. To regularize this inversion, we penalized deviations from the starting velocity model using an a priori model covariance matrix of the form

$$(\mathbf{C}_{\mathrm{m}})_{\mathrm{ij}} = \delta_{\mathrm{ij}}\lambda_{\mathrm{i}}^2, \tag{6}$$

where λ_{i}^2 is a weight equivalent to the a priori variance of the model parameters.

[13] To compare the results from different inversions, we estimated the root mean square (RMS) misfit of the resulting model and the variance reduction with respect to a uniform velocity model, $\mathbf{U_0}$. The RMS model misfit is defined as

$$\text{RMS misfit} = \sqrt{\frac{\left(\mathbf{U}^{\mathrm{obs}} - \mathbf{U}^{\mathrm{pred}}\right)^T\mathbf{C}_{\mathrm{d}}^{-1}\left(\mathbf{U}^{\mathrm{obs}} - \mathbf{U}^{\mathrm{pred}}\right)}{\mathrm{Tr}\left(\mathbf{C}_{\mathrm{d}}^{-1}\right)}}, \tag{7}$$

where $\mathrm{Tr}\,(\mathbf{C}_{\mathrm{d}}^{-1})$ is the trace or sum of the diagonal elements of $\mathbf{C}_{\mathrm{d}}^{-1}$, $\mathbf{U}^{\mathrm{obs}}$ are the observed values of $\mathbf{U}_{\mathrm{L}}$, and $\mathbf{U}^{\mathrm{pred}}$ are the values predicted by the model. The weighted variance reduction (ν) is

$$\nu = 1 - \frac{\left(\mathbf{U}^{\mathrm{obs}} - \mathbf{U}^{\mathrm{pred}}\right)^T\mathbf{C}_{\mathrm{d}}^{-1}\left(\mathbf{U}^{\mathrm{obs}} - \mathbf{U}^{\mathrm{pred}}\right)}{\left(\mathbf{U}^{\mathrm{obs}} - \mathbf{U_0}\right)^T\mathbf{C}_{\mathrm{d}}^{-1}\left(\mathbf{U}^{\mathrm{obs}} - \mathbf{U_0}\right)}. \tag{8}$$

2.2. Inversion for Shear Wave Velocity Structure

[14] We inverted the estimates of group velocity as a function of period to obtain the shear wave velocity V_{S} as a function of depth using the methodology described by *Villagómez et al.* [2007]. We performed inversions for one-dimensional structure for each dispersion curve by finding the best fit between the observed group velocities and those predicted by DISPER80 [*Saito*, 1988], which calculates

Table 1. Time Periods Used for Cross Correlation of Ambient Noise Records

Time Period	Number of Days	Stations Missing Data or With Data Gaps
6 Oct 1999 to 31 Oct 1999	26	G09
25 Nov 1999 to 5 Dec 1999	11	G09
18 Jan 2000 to 10 Feb 2000	24	G04 G07
1 Feb 2000 to 3 Mar 2000	32	G04 G07
5 Mar 2000 to 1 Apr 2000	28	G04 G07 PAYG
13 Apr 2000 to 19 May 2000	37	G07 G10
24 Jun 2000 to 6 Jul 2000	13	G03 G07 G10
18 Jul 2000 to 27 Aug 2000	41	G01 G03 G07 G10
5 Oct 2000 to 24 Oct 2000	20	G01 G07
5 Oct 2000 to 10 Nov 2000	37	G01 G07
19 Nov 2000 to 5 Dec 2000	17	G01 G07 PAYG
19 Jan 2001 to 12 Feb 2001	25	G01 G03 G07
2 Mar 2001 to 31 Mar 2001	30	G01 G03 G07
26 May 2001 to 22 Jun 2001	28	G01 G03 G07 G10
23 Sep 2001 to 18 Oct 2001	26	G07 PAYG
22 Oct 2001 to 10 Dec 2001	50	G07 PAYG
19 Dec 2001 to 10 Jan 2002	23	G07 G09 PAYG
11 Jan 2002 to 10 Feb 2002	31	G07 G09 PAYG
11 Feb 2002 to 1 Mar 2002	19	G07 G09
7 Mar 2002 to 22 Mar 2002	16	G07 G09
2 Apr 2002 to 25 Apr 2002	24	G01 G07 PAYG
27 Apr 2002 to 27 May 2002	31	G01 G04 G06 G07
4 Jun 2002 to 28 Jun 2002	25	G01 G04 G06 G07

normal modes for a laterally homogeneous model. The inversions solve for velocity perturbations from a starting model of V_S, P wave velocity V_P, and density ρ in an iterative process using the linearized inversion technique of *Tarantola and Valette* [1982]. Since group velocities of Rayleigh waves are mostly sensitive to changes in shear wave velocity and less to changes in V_P or density, we solved for changes to the V_S model, and then we converted these to V_P using a fixed V_P/V_S ratio at each iteration. We assessed the goodness of fit and compared the results of different inversions using the RMS misfit (equation (7)).

3. Results

3.1. Estimation of Group Velocity

[15] We applied the cross-correlation method to continuous vertical records from pairs of stations for 24 time periods that range from 11 to 50 days in duration between October 1999 and June 2002 (Table 1). The time periods were chosen in order to reduce the number of larger teleseismic events (surface wave magnitude $M_S > 7.0$), to avoid local swarms of earthquakes, and to maximize the number of stations available. We selected waveforms that had data gaps totaling less than 1 h during the span of each record. We subtracted a mean from and detrended each seismic record, and we then applied the one-bit normalization by replacing all positive amplitudes with 1 and all negative amplitudes with −1.

[16] Coherent wave trains emerged from the cross correlation of ambient noise (Figure 2). The wave trains are two sided, with amplitudes on either side varying in a manner dependent on the distribution of noise sources. *Sabra et al.* [2005] observed that for stations in southern California, given the network's vicinity to the Pacific coast, the cross-correlation wave trains are mostly one sided and the signal-to-noise ratio is higher for station pairs oriented perpendicular to the coast. For the Galápagos, in order to place the side of greater amplitude at positive lag, cross correlations between pairs of stations had to be performed using a southern then northern station order for any time period considered (for example, cross correlations of PAYG with G04, G05, G06 and G10; see Figure 2a), indicating that the noise sources were located to the south of the seismic network. In addition, there are no marked temporal variations in the relative amplitude of the two sides, a finding that suggests the noise sources were mostly stationary. However, the relative amplitude of the two sides of the signal varies with period (e.g., Figure 2b), indicating that the location of the noise sources may be frequency dependent. Additional analysis of amplitude variations with azimuth and period in a future study could help constrain the location of the sources of noise.

[17] At the station spacing in our network (between 65 and 250 km) the cross correlation is dominated by Rayleigh waves [*Shapiro and Campillo*, 2004; *Sabra et al.* 2005]. The group arrivals are easily seen on the cross corre-

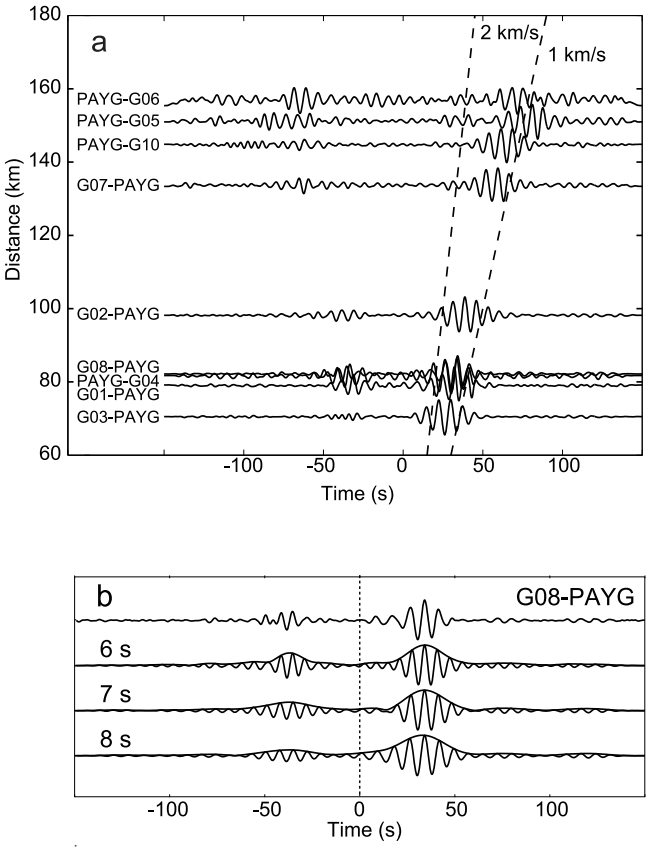

Figure 2. (a) Cross correlations of 26 days of seismic ambient noise records (6–31 October 1999) for pairs of stations that include PAYG. The horizontal axis is correlation lag time, and the vertical axis is the distance between stations. Dashed lines indicate velocities of 1 and 2 km/s. The sampling rate for all records was 20 Hz. (b) Unfiltered (top signal) and filtered signals (with envelopes) at periods of 6, 7, and 8 s for the G08-PAYG cross correlations shown in Figure 2a. The horizontal axis is the correlation time lag.

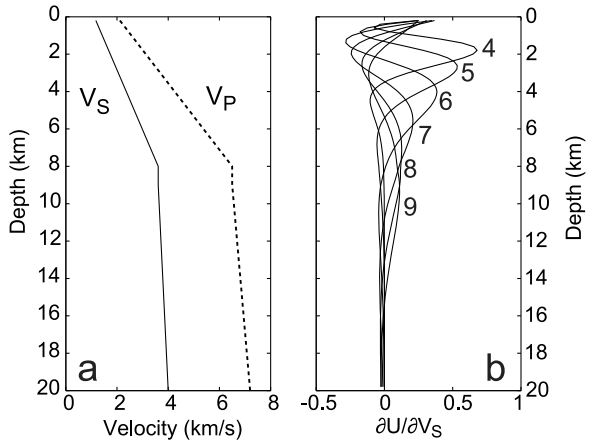

Figure 3. (a) Nominal model for V_P and V_S versus depth. (b) Sensitivity of Rayleigh wave group velocity to changes in V_S for the velocity model in Figure 3a, labeled by wave period in seconds.

lations, which predictably arrive later for stations separated by greater distances (Figure 2a). Filtering of the signal shows the dispersion of the Rayleigh wave velocity by period (Figure 2b). For the full data set, we obtained reliable measurements of group velocity for periods between 5 and 8.5 s, in the band of ocean-generated microseismic noise [*Friedrich et al.*, 1998]. Over this period band, the group velocity of Rayleigh waves is sensitive to V_S structure primarily between ~3 and ~10 km depth (Figure 3).

[18] Examples of group velocity measurements obtained with MFA are shown in Figure 4. We used the higher-amplitude half of the symmetric signal and filtered it with $\alpha = 25$ in equation (1) for periods between 2 and 12 s. The amplitude of the envelope was contoured as a function of period and group velocity, and the local maxima of the envelope are marked. Such plotting aids in the identification of the dispersion curve for the fundamental mode, which corresponds to the maximum amplitude, and helps to identify the range of periods where the signal is strongest. We chose only high-quality measurements where the amplitude is more than 50% of the maximum amplitude when estimating a dispersion curve. In addition, we required an interstation spacing (Δ) at least three times the wavelength (λ) [*Bensen et al.*, 2007]. The constraint $\Delta > 3\lambda$ is equivalent to $\Delta > 3UT$, where U is the group velocity and T is the period. For instance, group velocity measurements at greater than 7.5 s period for G01-G02 and at greater than 8.5 s period for G03-G08 were discarded because of small interstation spacing. MFA measurements of group velocity for two stations pairs, G02-G06 and PAYG-G05, for the time period between 1999/10/06 and 1999/10/31 are displayed in Figure 4. The resulting dispersion curves are also shown.

[19] We determined group velocity dispersion curves for all stations pairs and for all the time periods considered. Additionally, we stacked the cross correlations for each station pair, and we measured the group velocities from the stacked signal (Figure 5a). Stacking decreases the influence of potential seasonal variations in the source of noise and increases the signal-to-noise ratio of the cross correlation.

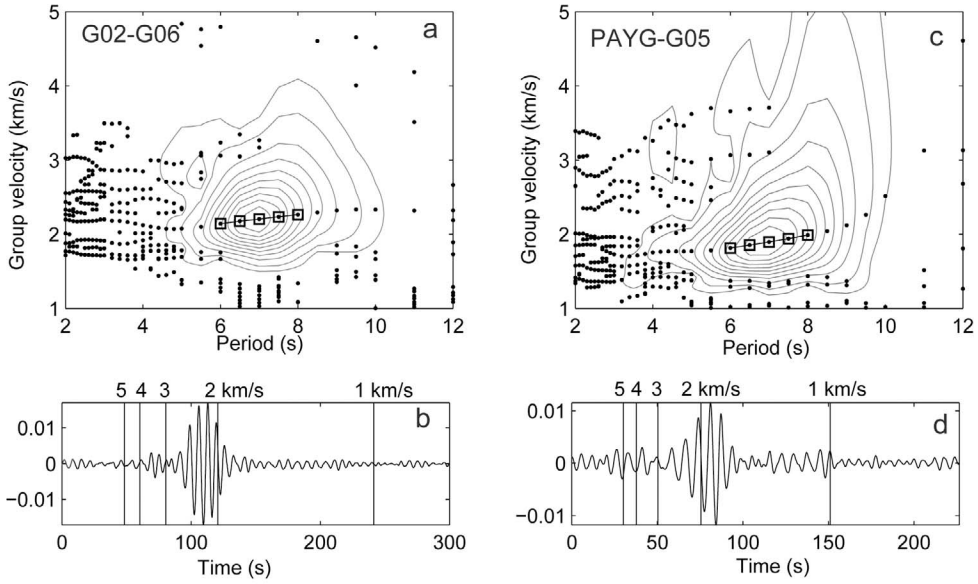

Figure 4. Results of multiple filter analysis (MFA) (http://www.eas.slu.edu/People/RBHerrmann/CPS330.html) performed on the positive side of the correlation time lag of two cross correlations (6–31 October 1999) for the station pairs: (a and b) G02-G06 and (c and d) PAYG-G05. Figures 4b and 4d show the unfiltered signal and the location in time of group velocity values from 1 to 5 km/s. Figures 4a and 4c show contours of the envelope of the filtered signal as functions of period and group velocity. Contours represent 10% to 90% (in increments of 10%) and 95% of the maximum amplitude of the envelope. Dots indicate locations of local maxima in the envelope. Lines with squares show the best estimates of the dispersion curves for fundamental mode Rayleigh waves.

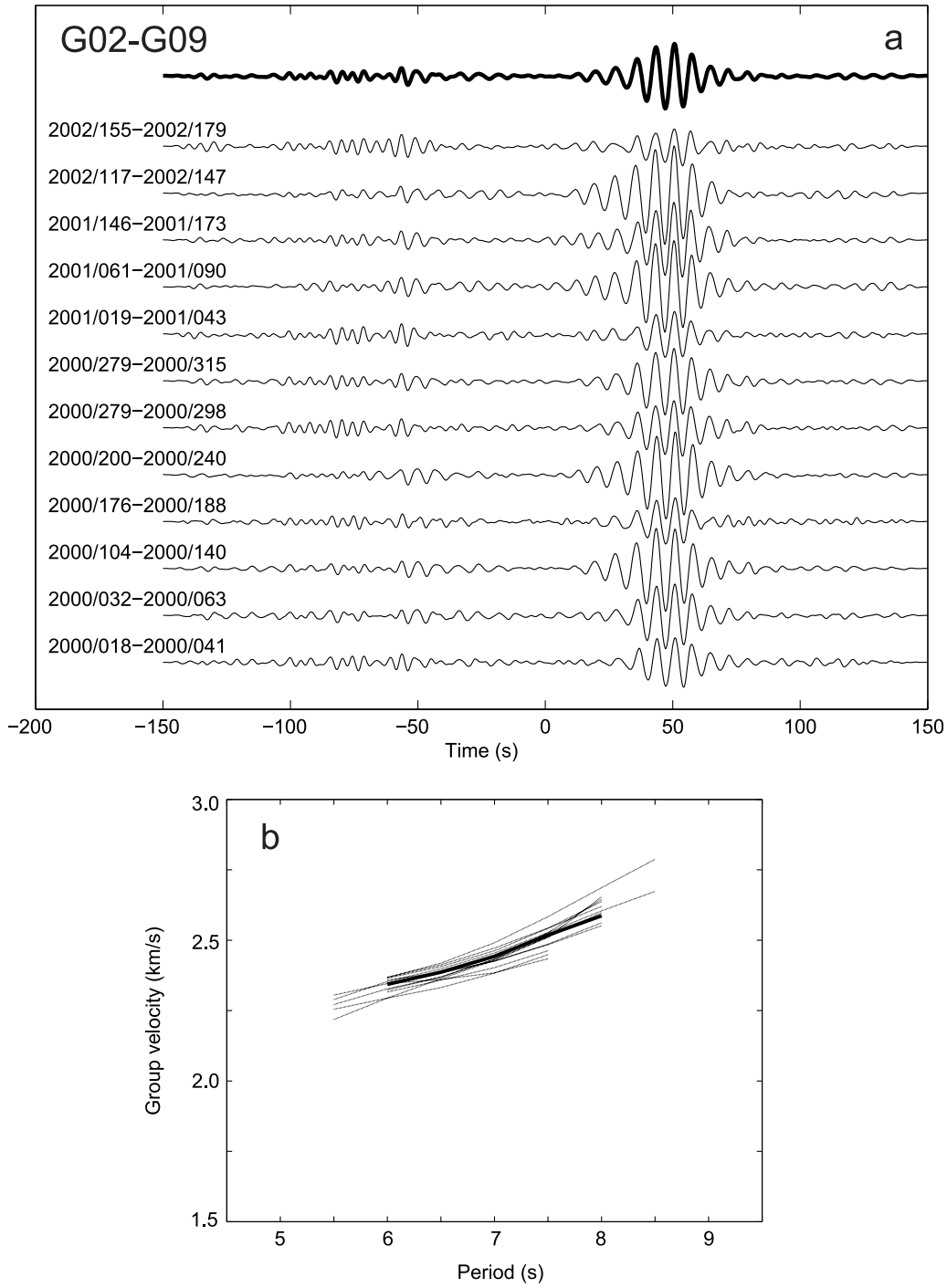

Figure 5. (a) Cross correlations of ambient seismic noise records between G02 and G09 for time periods shown to the left. Line on top shows the stacked signal resulting from taking the mean of all cross correlations. (b) Result of MFA performed on the right side of the cross correlations shown in Figure 5a at different time periods and on the stacked signal (thick line). The curves are truncated at low and high periods to keep only amplitudes greater than 50% of the maximum.

Notwithstanding such potential variations, multiple measurements of group velocity for each station pair at different time periods agree well (Figure 5b). A comparison of group velocities measured from individual time periods with the stacked signal provides an estimate of uncertainty arising from repeatability of the measurement. We estimate that the uncertainty in the group velocity is less than ±0.15 km/s.

[20] The distribution of seismic stations also allows us to test the accuracy of some of the group velocity measurements. When three or more stations are aligned, it is possible to estimate the group velocity along any of the subpaths given the velocities along the other subpaths. For instance, stations G03, PAYG, and G09 are nearly aligned (Figure 6a), and thus the group delay at a given period for the

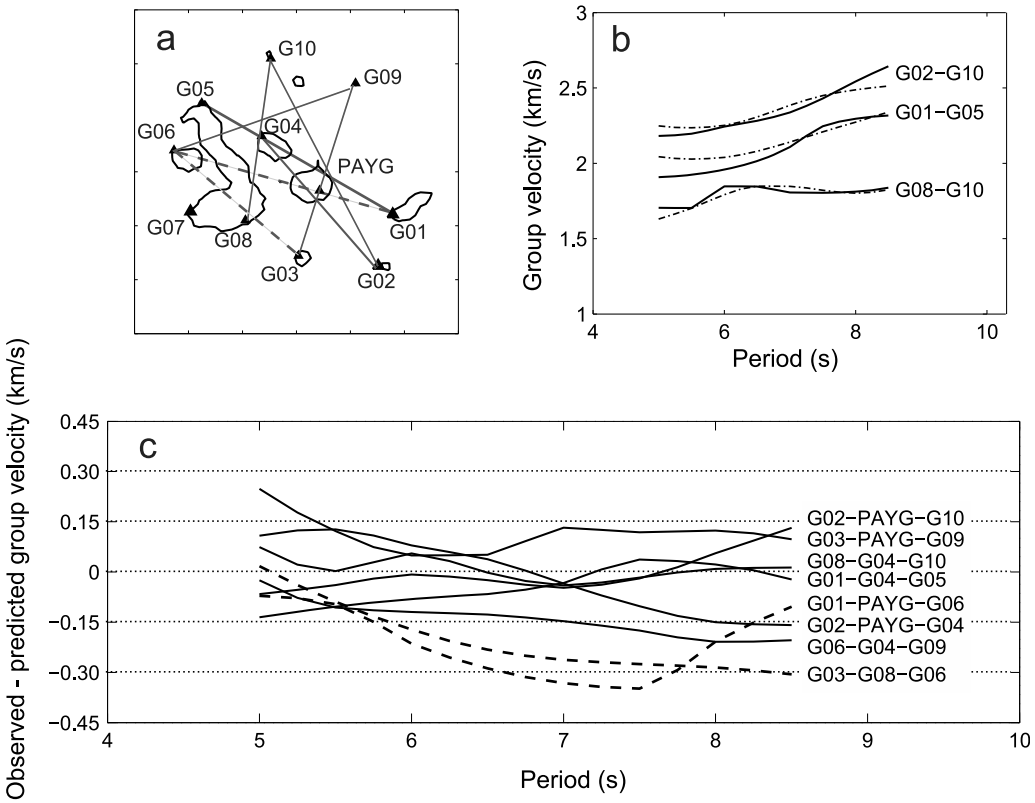

Figure 6. Group velocity analysis for paths along which three stations are nearly aligned. (a) Locations of the stations and paths represented. (b) Comparison of predicted (dashed-dotted lines) and observed (solid lines) group velocities for selected paths as a function of period (see text for further explanation). (c) Predicted minus observed group velocities for all paths shown in Figure 6a. Dashed lines in Figures 6a and 6c indicate paths with larger discrepancies between predicted and observed values.

path G03-G09 can be estimated from the sum of the group delays for the subpaths G03-PAYG and PAYG-G09. Group velocities obtained by this method can then be compared to the observed velocities. We found eight different near alignments of three stations in our data set. Values of the group velocity predicted with this method are compared to the observed velocity for three of these paths in Figure 6b, and values of the discrepancy between the predicted and observed velocities for all eight paths are shown in Figure 6c. This discrepancy for a three-station path can be taken as a measure of the combined accuracies of the group velocity estimates for each of the subpaths. Over the period range 5 to 8.5 s, six out of the eight paths show discrepancy values that fall mostly within ±0.15 km/s (Figure 6c), consistent with our previous estimate of 0.15 km/s for the group velocity uncertainty. The remaining two paths (G01-PAYG-G06 and G03-G08-G06, dashed lines in Figure 6c) show discrepancy values that fall mostly within ±0.3 km/s, still within the range of differences expected when three measurements with uncorrelated uncertainties of 0.15 km/s are combined.

[21] The average of the measurements for all station pairs gives us an average group velocity dispersion curve for the entire Galápagos platform (Figure 7a). We computed the uncertainty of this measurement as a function of period by taking the RMS of all the individual station pair uncertainties. We used only those periods where the number of high-quality paths exceeded 10 (out of the possible 55), a criterion satisfied by the periods between 5 and 8.5 s (Figure 7b). Figure 7a shows that the average Rayleigh wave group velocity increases from 1.81 km/s to 2.33 km/s between periods of 5 and 8.5 s. The estimated uncertainties vary between 0.1 and 0.2 km/s (Figure 7a).

[22] Compared with the average velocity, the group velocities between pairs of stations in the western archipelago are generally lower than those in the eastern archipelago (Figures 8 and 9). For example, the paths G04-G05, G05-G06, and G05-G07 in the western archipelago have group velocities that are 0.3–0.7 km/s lower than the average at all periods, while the paths G01-G03, G02-G09, and G09-PAYG in the eastern archipelago have group velocities that are 0.3–0.4 km/s higher than the average (Figure 8). The differences in group velocities between the paths in the western and eastern archipelagos are 4 to 6 times larger than the estimated uncertainty in the measurement (0.15 km/s). Figure 9 shows all the paths between station pairs for periods between 5 and 8 s, with red lines indicating group velocities lower than the average, and blue higher than average. The difference between the eastern and western archipelago is substantial, with variations in group velocity of up to ±30% from the average (Figure 9).

[23] To determine lateral variations in group velocity structure, we inverted the group velocity measurements for all station pairs at eight different periods (from 5 to 8.5 s).

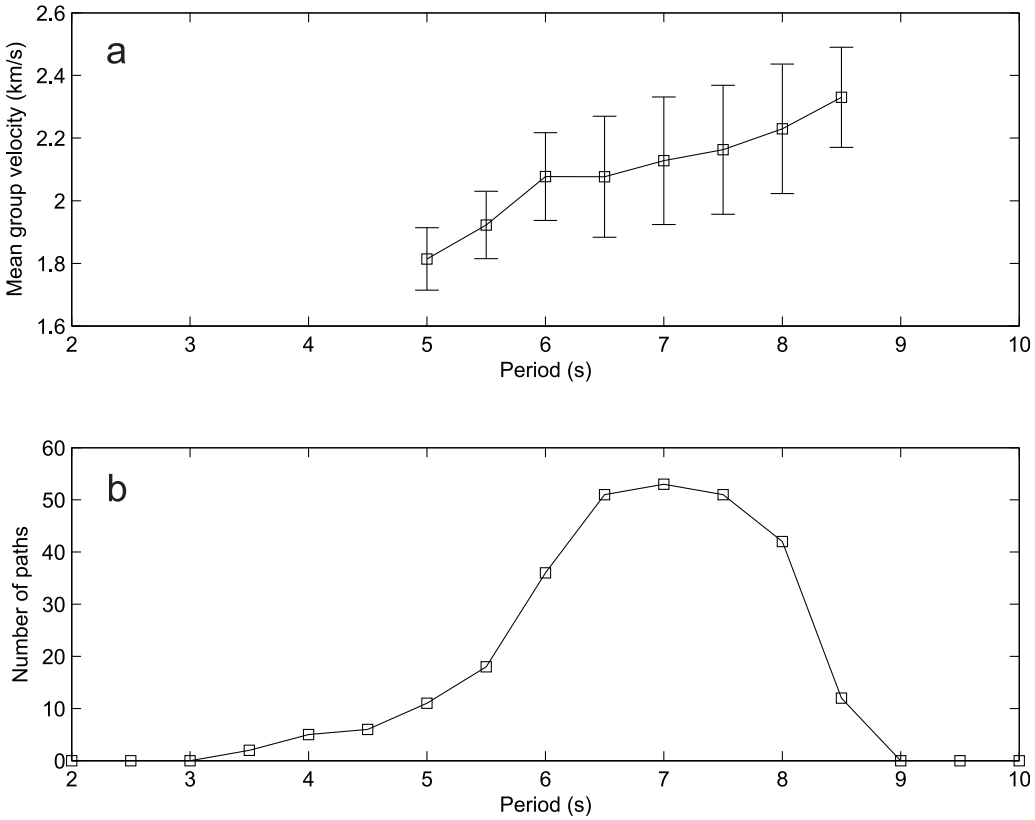

Figure 7. (a) Average dispersion curve for the entire archipelago computed from MFA results from station pair stacked cross correlations. Error bars indicate one standard deviation. (b) Number of station pairs used to calculate the mean as a function of period.

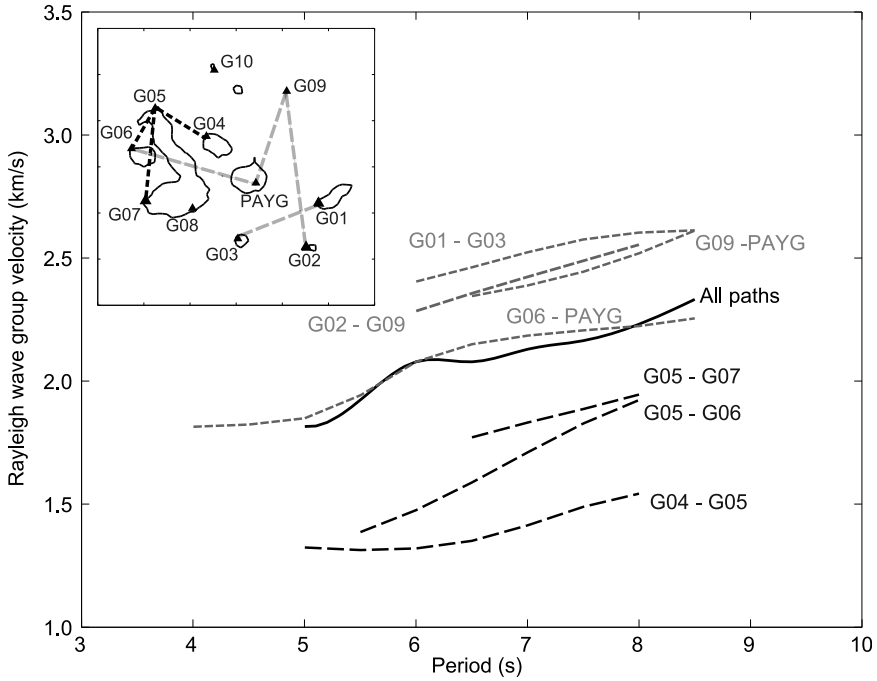

Figure 8. Smoothed dispersion curves for selected station pairs compared with the average for the region (thick black line). The inset shows the locations of the stations and paths represented.

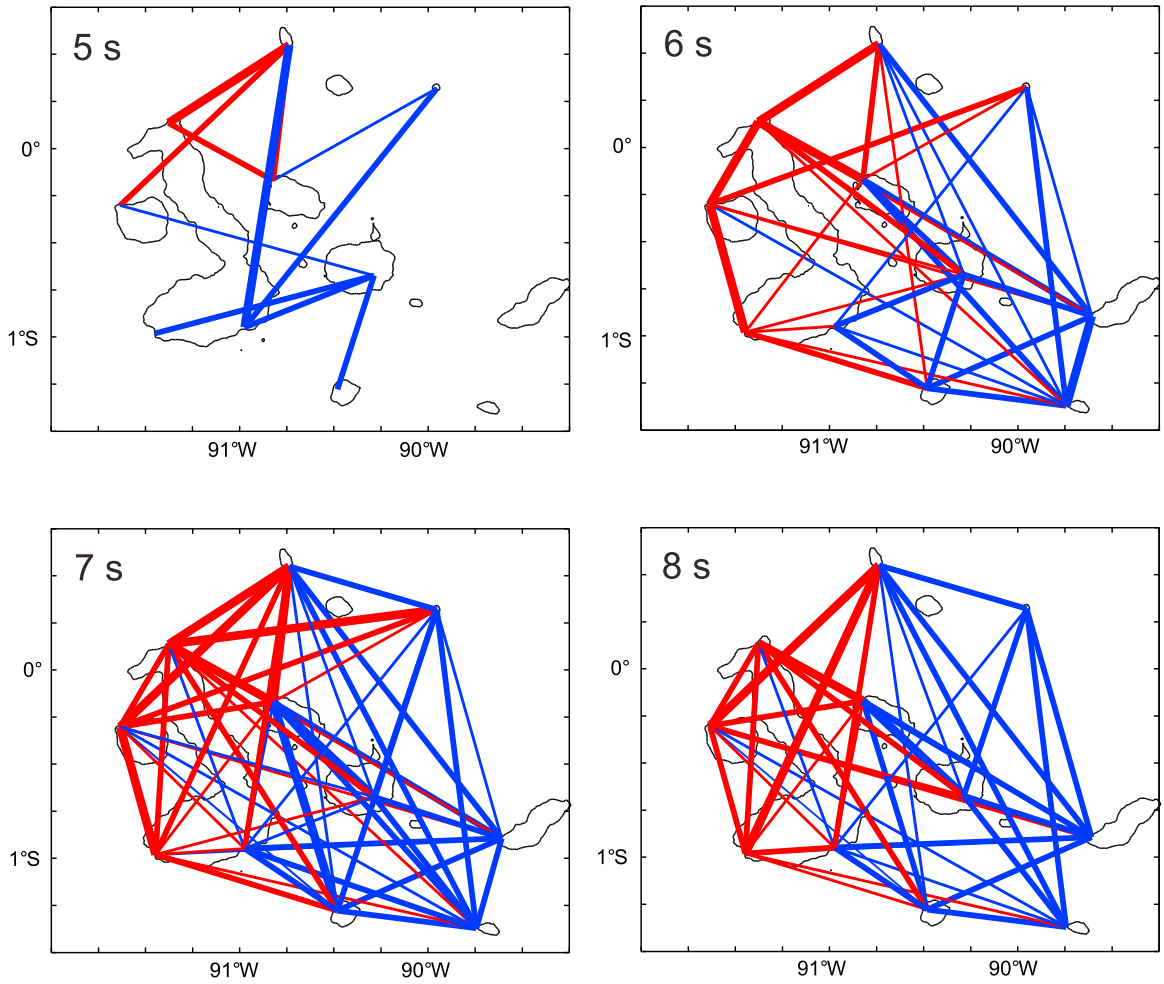

Figure 9. Maps of paths along which group velocity measurements were determined at periods between 5 and 8 s. Red colors indicate that the group velocity is less than the average velocity, whereas blue colors indicate velocities higher than average. Thickness of the line is proportional to the difference from the average group velocity.

We used the average dispersion curve in Figure 7a as the starting model in the inversions, and we parameterized the region with two-dimensional blocks. In initial inversions the region was parameterized as two blocks, one each in the eastern and western parts of the archipelago (Figure 10a). We found the velocities with a damped least squares approach with $\beta = 0.1$ in equation (4), and we estimated model uncertainties with a Monte Carlo sampling approach [e.g., *Metropolis and Ulam*, 1949; *Mosegaard and Tarantola*, 1995] by repeating each inversion 100 times using different input station-to-station group velocities drawn randomly from a Gaussian distribution with a variance appropriate to the estimated uncertainty in the observations.

[24] The results of the inversion show a clear distinction between the western and eastern blocks (Figure 10b). Group velocities in the western block are 40–50% lower than in the eastern block. Moreover, the variance reduction of using two blocks compared to a uniform velocity model is 63% (total RMS misfit = 0.29 km/s), indicating that most of variability in the observations is due to differences between the eastern and western archipelago.

[25] We next parameterized the region with four blocks (southwestern or SW, southeastern or SE, northwestern or NW, and northeastern or NE) to investigate north–south differences in group velocity (Figure 10c). We again used a damped least squares approach with $\beta = 0.1$. The results show that the northern blocks are about 15–25% lower in average group velocity than their respective southern blocks (Figure 10d). The northwestern archipelago is the lowest-velocity region, with group velocities that are 25–45% lower than the average, while the southeastern archipelago is the highest-velocity region, with velocities that are 10–25% higher than the average. The variance reduction obtained using this model with respect to a uniform velocity model is 78% (total RMS misfit = 0.25 km/s), suggesting that there are important variations in group velocity in the north–south direction.

[26] We then ran inversions using blocks of width 0.25° in latitude and longitude. Because damped least squares does not guarantee the positivity of the solution in each block, we parameterized the group velocity (U) in terms of $r = \ln(U)$ and used an iterative inversion [e.g., *Wilcock et al.*, 1995].

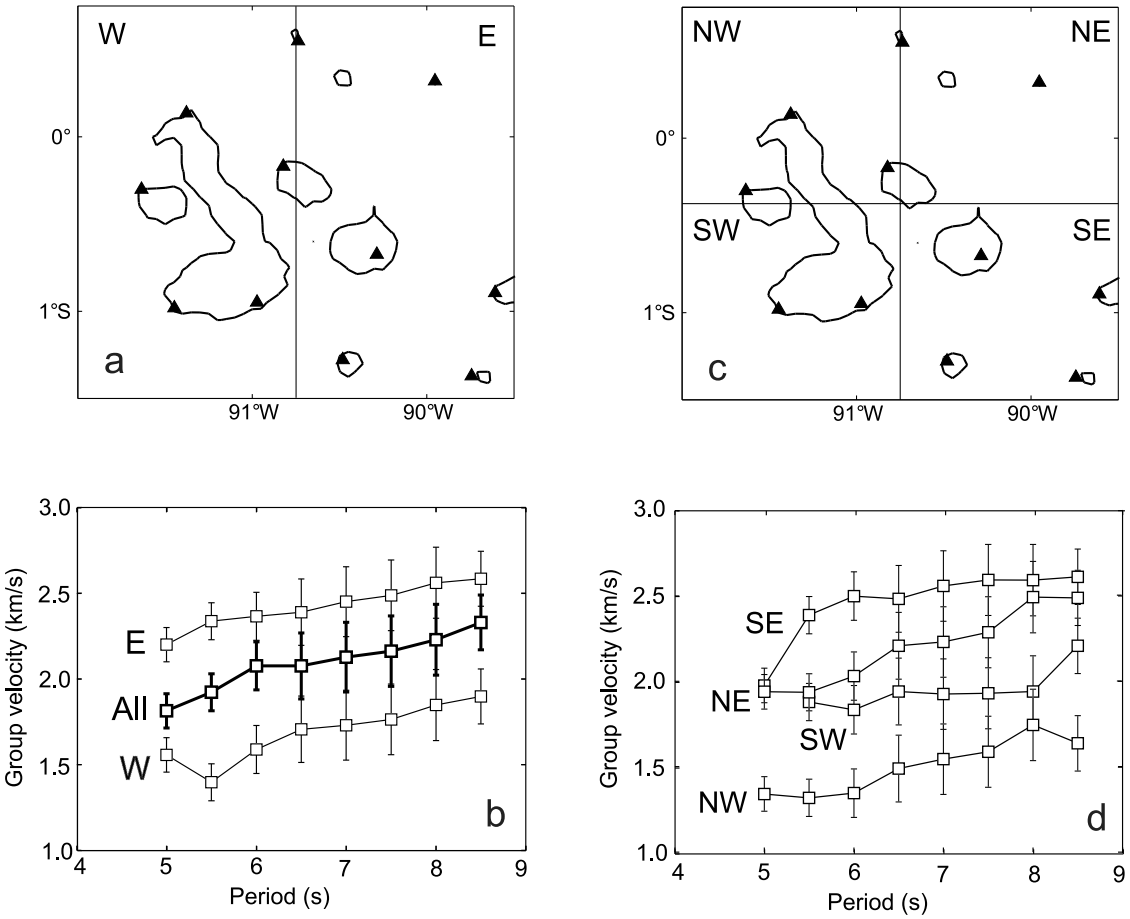

Figure 10. (a and b) Results of group velocity inversions when the region is divided into the two blocks shown in Figure 10a. In Figure 10b, dispersion curves for the two blocks (gray) are compared with the average dispersion curve (black). (c and d) Results of group velocity inversions when the region is divided into the four blocks shown in Figure 10c. Figure 10d shows dispersion curves for the four blocks. Error bars represent one standard deviation.

Inversions with λ_i varying between 0.01 and 0.5 show misfit varying from 0.18 to 0.12 km/s (variance reduction from 81% to 97%, respectively). The results of these inversions are consistent with those of the previous inversions, with the lowest group velocities in the northwestern archipelago.

[27] This area lowest group velocities coincides with a region of deep seafloor (greater than 2000 m) (Figure 1), suggesting that water depth could be responsible for some of the low group velocities observed. This inference is consistent with the observation that the paths G04-G05, G05-G10, and G04-G10 show some of the lowest measured group velocities ($U < 1.5$ km/s) in our data set (Figures 8 and 9). By way of example, Figure 11 shows the effect on the group velocity when water columns of thickness 750 m and 2000 m ($V_P = 1.5$ km/s, $V_S = 0$, $\rho = 1000$ km/m^3) are added to the top of an assumed velocity model. The addition of a water column having a thickness of up to 2000 m has the effect of decreasing the group velocity estimates for periods less than about 12 s.

[28] We conclude that most of the variance reduction was gained in the first inversion with two blocks, so the greatest spatial variability of seismic velocities is in the east–west direction. However, our inversion procedure cannot determine if the group velocity increase observed from west to east is gradual or abrupt. To address this issue, we estimated average group velocities for each station and analyzed their variations by longitude (Figure 12). We calculated the averages using all the station pair group velocities associated with a particular station. We found that the group velocity gradually increases from west to east. The average rate of increase from the best fitting line is 0.21 km/s per degree of longitude at 6 s period and 0.31 km/s per degree at 8 s period.

[29] To study the possible effects of crustal azimuthal anisotropy on the propagation of Rayleigh waves, we analyzed the group velocity residuals for a potential cos (2θ) dependence, where θ is the azimuth clockwise from north of the station pair path. We found no dependence, suggesting either that the crust is azimuthally isotropic or that azimuthal anisotropy cannot be resolved with the current data set.

3.2. Inversions for V_S

[30] We inverted the average dispersion curve and those of the different subregions (Figure 10) to obtain profiles of V_S versus depth. The models are parameterized in increments of 250 m depth between 0 and 20 km. For the starting

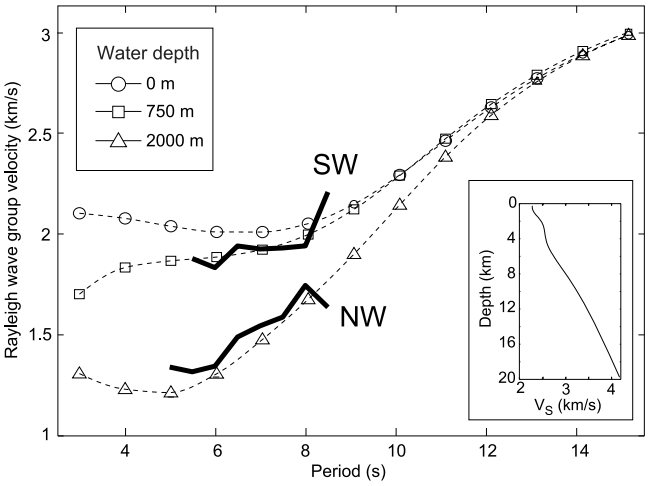

Figure 11. Effect on the group velocity (dashed lines) of adding a column of water (V_P = 1.5 km/s, V_S = 0 km/s) to the top of the velocity model shown in the inset. Circles indicate no water column, squares indicate a 750 m deep water column, and triangles indicate a 2000 m deep water column. Thick lines show the observed group velocities for the SW and NW blocks.

model and during the inversion we used a constant ratio of V_P/V_S = 1.8, and we approximated density from ρ (kg/m^3) = 3810 – 6000/V_P [*Carlson and Herrick*, 1990]. Although V_P/V_S likely varies with depth, the inversion is more sensitive to changes in V_S than to V_P or density, so different choices of V_P/V_S or density do not markedly change the results.

[31] For each inversion, we estimated uncertainties in V_S with a Monte Carlo sampling approach [e.g., *Metropolis and Ulam*, 1949; *Mosegaard and Tarantola*, 1995] by repeating each inversion 50 times with input group velocities drawn randomly from a Gaussian distribution having a variance appropriate to the estimated uncertainty in the observations. We also analyzed the effects of changing the starting model by comparing the inversion results for nine different starting models (dashed lines in Figure 13a). We show the range of results of the V_S inversions as shaded areas, which represent the resulting average V_S models together with two standard deviation uncertainties ($2\sigma_v$). For all inversions we assumed a prior uncertainty in velocity model parameters of 0.3 km/s and a smoothing length of 7.5 km [see *Villagómez et al.*, 2007]. Table 2 shows the average RMS misfit of the inversions and the estimated water depths for each region.

[32] We first inverted the average dispersion curve shown in Figure 7a. Figure 13a gives the range of results from the inversions and shows that regional V_S increases from 2.53 ± 0.08 km/s at 3 km depth to 3.23 ± 0.14 km/s at 10 km depth. The uncertainty in V_S is lowest between about 3 and 10 km depth (σ_v = 0.06 – 0.14 km/s). This behavior is also illustrated in Figure 13b, which shows that resolution for the period range considered here is best between 3 and 10 km depth (horizontal lines in Figure 13a), is poor shallower than ~2 km depth, and decreases rapidly with depth for depths greater than ~10 km.

[33] The number of observations in the inversion (n = 8) indicates that we can potentially recover a maximum of eight pieces of information about the V_S model. However, the observed group velocities are not independent observations. The trace of the resolution matrix, Tr (**R**) = 1.8, shows that we can only recover ~2 independent pieces of information about the model. To examine the dependence of different model parameters on information at adjacent layers, we inspect the rows of the resolution matrix (Figure 13c). For

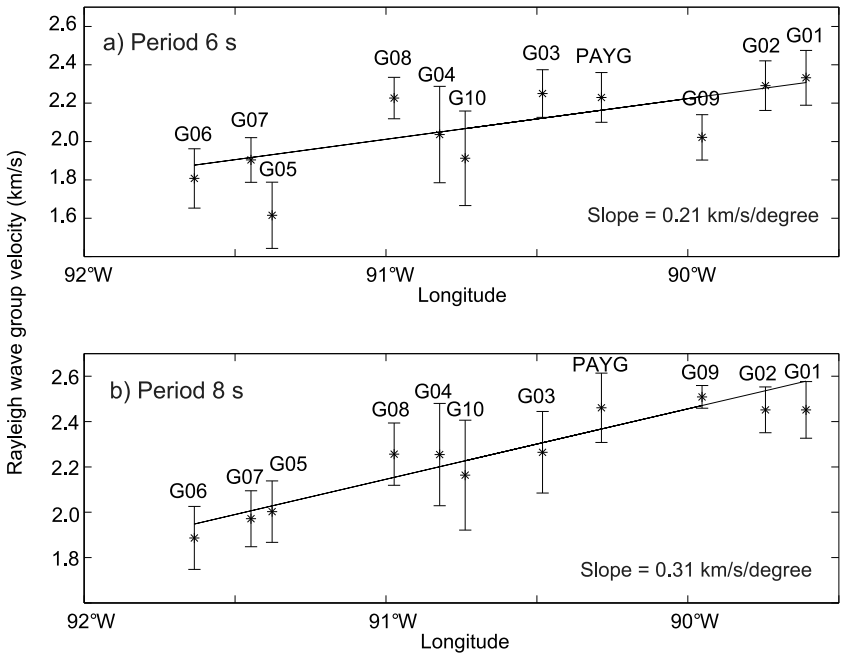

Figure 12. Average value of Rayleigh wave group velocity for each station at a period of (a) 6 s and (b) 8 s, plotted as functions of longitude. The averages are calculated from the group velocities measured for all station pairs that include the respective station. Error bars indicate one standard deviation.

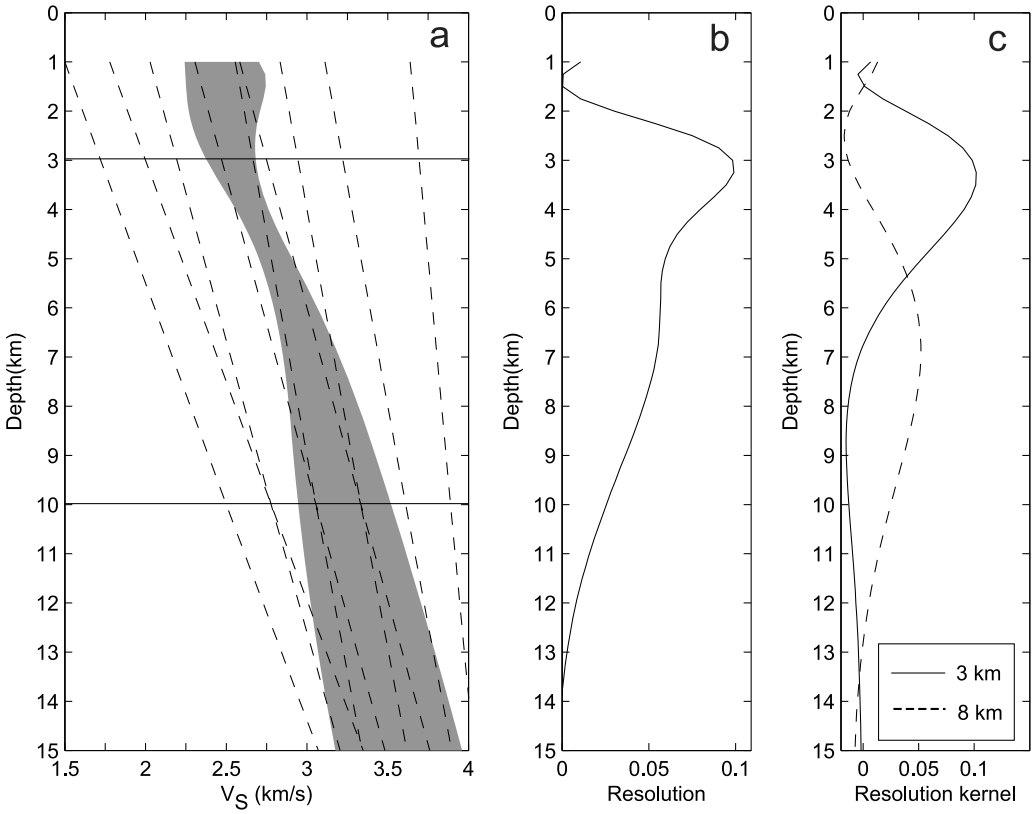

Figure 13. Results of inversions for V_S of the regional average Rayleigh wave group velocity (Figure 7a). (a) The shaded area shows average V_S from the inversions, together with its two standard deviation uncertainty, as a function of depth. Dashed lines indicate starting velocity models for the inversions. Horizontal lines delimit the depth range of best resolution. (b) Resolution (diagonal elements of resolution matrix) as a function of depth. (c) Resolution kernels (rows of the resolution matrix) at depths of 3 and 8 km.

instance, the value of V_S recovered at 8 km depth is a weighted average of seismic structure between ~3 and 12 km depth (dashed curve in Figure 13c), whereas the value of V_S at 3 km depth is a weighted average of structure in the upper ~7 km (solid curve in Figure 13c).

[34] The results of inverting the dispersion curves for the western and eastern archipelago are compared in Figure 14. The results show a substantial difference in V_S structure between the eastern and western parts of the archipelago at least from 3 to 7 km depth. V_S beneath the western archipelago is 12–25% lower than that beneath the eastern archipelago at 3 km depth, and 5–20% lower at 7 km depth. On average, crustal V_S beneath western archipelago is 15% lower than that beneath the eastern archipelago between 3 and 10 km depth.

[35] Within the western part of the archipelago, group velocities are markedly lower in the NW block than in the SW block (Figure 10d). We suggest that this difference in group velocity may be entirely the result of the difference in water depth. Across the NW block water depth averages ~2000 m, whereas it is ~750 m in the SW block. As seen in Figure 11, group velocities for both the SW and NW blocks can be fit relatively well using the same velocity model (Figure 11 inset) except for different thicknesses of the water layer.

[36] The results of the inversions for the SE and NE blocks are shown in Figure 15. Crustal V_S in the NE block is on average up to 5% lower than in the SE block between 3 and 10 km depth. Seismic velocity is most different at 5 km depth, where V_S in the NE block is ~0–12% lower than that in the SE block. However, these differences do not exceed the uncertainties in the recovered model parameters.

4. Discussion

4.1. Crustal Structure

[37] Crustal velocities beneath the Galápagos are lower than those of very young oceanic crust at the East Pacific Rise (EPR), and comparable to those of Hawaii (Figure 16). Figure 16a shows a comparison of V_P (under the assumption

Table 2. RMS Misfit of Inversions for V_S

	RMS Misfit (km/s)	Water Layer (m)
Entire archipelago	0.1207	1000
Western (W)	0.1419	1250
Eastern (E)	0.1163	1000
Southeastern (SE)	0.1770	1000
Northeastern (NE)	0.1352	1250

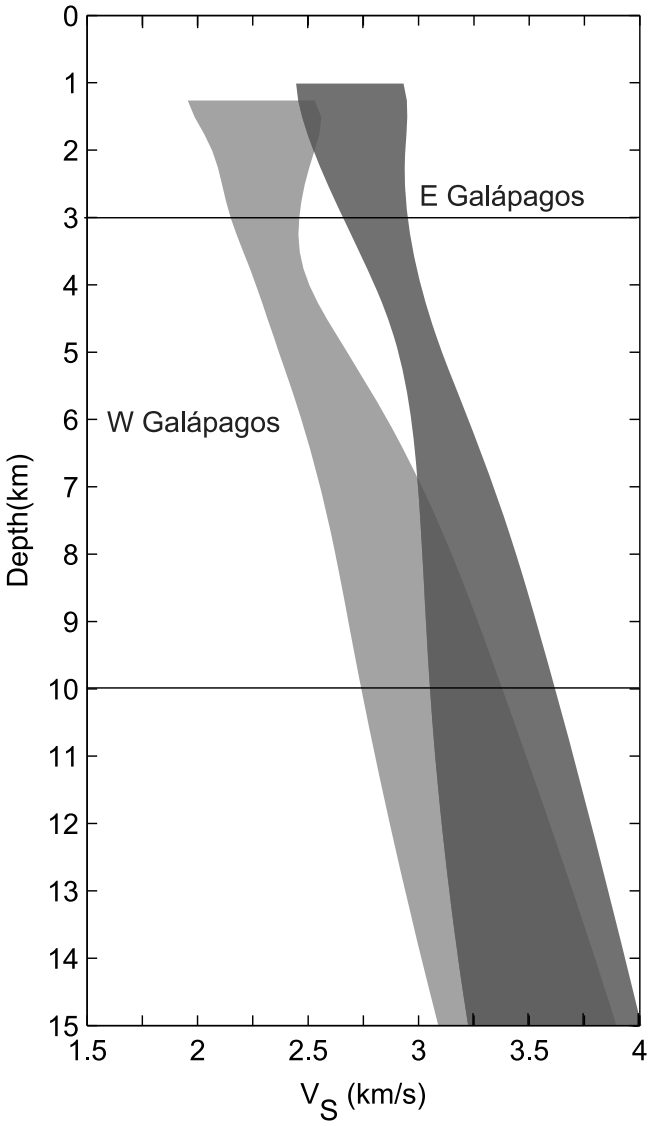

Figure 14. Results of inversions for V_S of Rayleigh wave group velocity for the eastern and western archipelagos. The shaded areas show average V_S from the inversions, together with their two standard deviation uncertainties, as functions of depth. Horizontal lines delimit the depth range of best resolution.

that $V_P/V_S = 1.8$) as a function of depth relative to sea level for the Galápagos Archipelago, 0–200 ky old crust at 9°N at the EPR [*Vera et al.*, 1990], and 150–350 ky old crust on the eastern and western sides of the EPR (at 9°10′N for the outer western profile and at 9°50′N for the outer eastern profile of *Canales et al.* [2003]). Crustal V_P inferred beneath the Galápagos is up to 20% lower than the western side of the EPR, and up to 25% lower than either 0–200 ky old EPR crust or the eastern side of the EPR (Figure 16a). The difference in V_P between the Galápagos and the EPR is still substantial if V_P/V_S is taken to range from as low as 1.6 to as high as 2.0 (by as much as 45% and 15%, respectively), either for a constant V_P/V_S or allowing that ratio to vary with depth.

[38] Compared with a one-dimensional V_P profile for southern Hawaii [*Klein*, 1981], crustal V_P inferred for the Galápagos Archipelago is similar between 3 and 9 km depth (Figure 16b). In contrast, crustal V_P beneath the eastern archipelago is up to 8% lower than that of the western Carnegie Ridge at ~85°W, 250 km east of the Galápagos hot spot [*Sallarès et al.*, 2005], and up to 10% lower than that determined at Oahu, 200 km from the center of the Hawaiian hot spot [*Ten Brink and Brocher*, 1987] (Figure 16b).

[39] We suggest that the lower than normal crustal seismic velocities beneath the Galápagos are caused by a combination of heating by increased intrusive activity in the lower crust due to the injection of hot spot–derived magmas and the construction of a highly porous volcanic platform

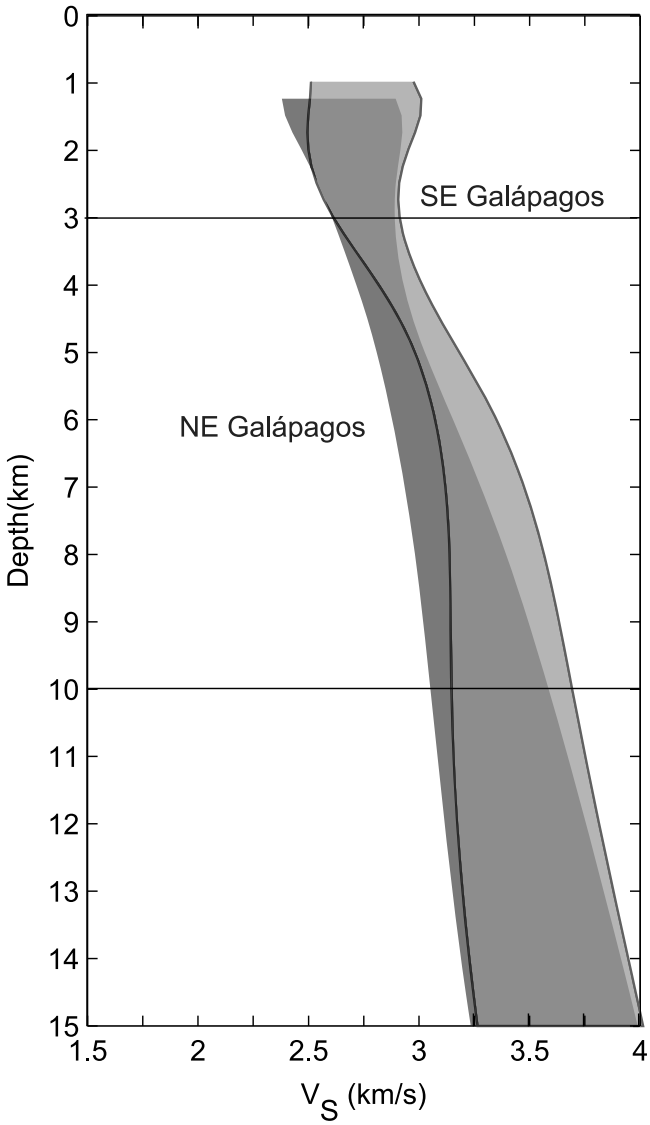

Figure 15. Results of inversions for V_S of Rayleigh wave group velocity for the northeastern (NE) and southeastern (SE) parts of the archipelago. Shared areas show V_S together with its two standard deviation uncertainty as a function of depth. Horizontal lines delimit the depth range of best resolution.

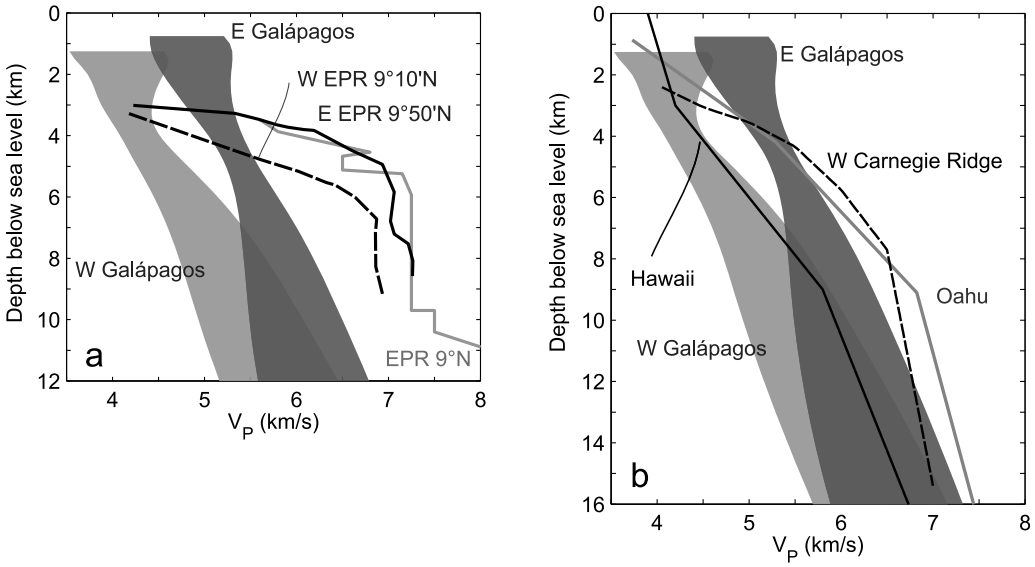

Figure 16. Comparison of crustal V_P models beneath the western and eastern Galápagos computed from V_S using $V_P/V_S = 1.8$ (shaded areas) with (a) estimates for 0–200 ky old crust at 9°N along the EPR (gray line) [*Vera et al.*, 1990] and of 150–350 ky old crust on both the eastern and western (E and W, solid and dashed black lines, respectively) sides of the EPR (at 9°10′N for the outer western profile and at 9°50′N for the outer eastern profile of *Canales et al.* [2003]), and (b) those estimated beneath the western Carnegie Ridge (dashed line) [*Sallarès et al.*, 2005], southern Hawaii (solid black line) [*Klein*, 1981], and Oahu (solid gray line) [*Ten Brink and Brocher*, 1987]. V_P profiles are shown as a function of depth below sea level.

emplaced on top of the preexisting oceanic crust. These combined effects are responsible for the thickening of the crust beneath the Galápagos from ~6 km to the west of the archipelago to ~16 km near the center [*Feighner and Richards*, 1994; *Toomey et al.*, 2001].

[40] There is a marked variation in crustal velocities within the archipelago. V_S beneath the western archipelago is up to 15% lower than beneath the eastern archipelago at 3–10 km depth (Figure 14). This difference is consistent with results from surface wave tomography [*Villagómez et al.*, 2007] that show lower than normal seismic velocities beneath the western archipelago extending to 40 km depth. The west-to-east increase in seismic velocities seems to be gradual (Figure 12). This velocity increase correlates well with distance downstream from the hot spot, and our observations give an increase of Rayleigh wave group velocity of 0.04–0.06 km/s, or about 2–3% per million years, at 6–8 s period (for a velocity of the Nazca plate of 21 mm/y at 0°N, 91°W [*Gripp and Gordon*, 2002], and an average Rayleigh wave group velocity of 2.0 km/s).

[41] We attribute the lower seismic velocities observed in the western crust to a combination of higher temperatures and higher amounts of melt at middle- to lower-crustal depths and to higher porosity within the extrusive rocks. We suggest that the western crust is warmer than the eastern crust, particularly at greater depths, because it lies above the inferred position of the Galápagos mantle plume [*Toomey et al.*, 2002; *Hooft et al.*, 2003; *Villagómez et al.*, 2007]. However, the difference in seismic velocity between the western and eastern crust is too large to be attributed solely to temperature. For instance, for $\partial \ln V_P/\partial T = -14 \times 10^{-5}$ K^{-1} [e.g., *Dunn et al.*, 2005], a 15% difference in seismic velocity at 3–10 km depth would imply a 1100 K difference in temperature.

[42] Larger amounts of melt within the crust of the western archipelago can account for some of the observed velocity anomaly. The western archipelago is the location of the youngest and most active volcanoes in the region [*McBirney and Williams*, 1969; *White et al.*, 1993]. Also, the western volcanoes are likely underlain by long-lived magma chambers [*Geist et al.*, 1998], and some of them may overlie a thick column of gabbroic mush that extends to the Moho [*Geist et al.*, 2005]. In contrast, the eastern volcanoes have experienced only a few Holocene eruptions, and petrologic evidence suggests that they do not have long-lived crustal magma chambers [*Geist et al.*, 1998]. If the melt-containing regions beneath the western volcanoes have horizontal extents comparable to those of the overlying calderas, only about 15–25% of the lengths of the paths between western seismic stations cross these melt regions. If solely attributed to melt beneath calderas, a 15% difference in seismic velocity at 3–10 km depth would imply a 60–100% velocity reduction in the regions influenced by crustal melt. Alternatively, our results could be consistent with more modest amounts of partial melt if a larger horizontal extent of the crust is partially molten.

[43] A complementary explanation for the lower velocities observed in the western archipelago is that they reflect increased porosity of the extrusive layers. Porosity is one of the most important factors controlling seismic velocity in the uppermost oceanic crust [e.g., *Spudich and Orcutt*, 1980; *Shaw*, 1994]. Beneath the Galápagos, the east–west differ-

ence in velocity is somewhat larger in the upper parts of the crust (12–25% lower V_S at 3 km depth compared to 5–20% lower V_S at 7 km depth), where higher volumetric fractions of extrusive rocks are expected.

[44] We attribute the west–to–east crustal velocity increase with age between 3 and 9 km depth to a combination of cooling of the crust after its passage above the Galápagos plume and a gradual decrease in porosity of extrusive rocks as a result of compaction, closing of cracks, and filling of open void spaces with hydrothermally deposited minerals [e.g., *Grevemeyer and Weigel*, 1997]. A west-to-east decrease in the amount of melt present in the crust, inferred from the apparent absence of long-lived crustal magma chambers beneath the eastern volcanoes [*Geist et al.*, 1998], is likely also to contribute to the eastward velocity increase, although this source of change may not be gradual. *Geist et al.* [1998] proposed two explanations for the systematic variation in the depth of magma chambers in the region: the depth is controlled by the rate at which magma is supplied from the mantle as the crust is carried away from the plume, or the depth is controlled by regional differences in lithospheric structure [e.g., *Feighner and Richards*, 1994]. The former explanation would be expected to lead to a gradual variation in characteristics influenced by crustal melt, whereas the latter explanation could yield either gradual or abrupt variations in crustal properties depending on the form of the lithospheric structure variations (see also section 4.2).

[45] Farther downstream from the hot spot, beneath the western Carnegie Ridge, 250 km east of the Galápagos, the average crustal seismic V_P [*Sallarès et al.*, 2005] is higher than that beneath the archipelago at depths greater than ~4 km (Figure 16b). At 8 km depth, V_P beneath the western Carnegie Ridge is 8–16% higher than that inferred beneath the eastern Galápagos Archipelago, equivalent to a V_P increase of about 0.7–1.3% per million years during the last 12 million years (for a Nazca plate velocity of 21 mm/y and 250 km distance). With $\partial \ln V_P/\partial T = -14 \times 10^{-5}$ K^{-1} [e.g., *Dunn et al.*, 2005], the V_P increase represents a temperature decrease of ~50 K per million years if attributed solely to temperature. We suggest that this west–to–east velocity increase, like that observed within the archipelago, represents mostly a combination of cooling and a decrease in porosity. A pattern of crustal velocity increase with age is also observed at the Hawaiian Islands between southern Hawaii and Oahu (Figure 16b).

4.2. Lithospheric Strength

[46] A distinctive characteristic of the Galápagos platform is its large spatial variation in lithospheric strength. From gravity, geoid, and bathymetry data, *Feighner and Richards* [1994] determined that the western and southern parts of the archipelago are underlain by elastically competent lithosphere, but the flexural rigidity of the northeastern archipelago is at least 1 order of magnitude smaller. *Feighner and Richards* [1994] attributed this pattern to (1) reheating of the northeastern lithosphere by the plume, (2) an age offset of the lithosphere resulting from the 91.5°W Galápagos Fracture Zone (GFZ), and/or (3) differing elastic strength at the time of loading. Because elastic strength strongly correlates with the thermal state of the lithosphere [e.g., *Watts and Zhong*, 2000], our V_S results, which broadly constrain the spatial variations in the present thermal structure of the crust, can be used to test possible explanations.

[47] The first explanation, that the elastic thickness in the eastern archipelago was reduced because of reheating by plume material advected eastward with plate motion requires the eastern lithosphere to be warmer, which is inconsistent with the results presented here. Moreover, results of surface wave tomography show no evidence of thermal erosion of the eastern lithosphere [*Villagómez et al.*, 2007], so this alternative may be ruled out.

[48] The second explanation suggests that the boundary separating elastically competent lithosphere in the west from Airy isostasy in the east (Figure 17) corresponds to an age discontinuity created by the GFZ, and thus requires the GFZ to extend southward to at least 1°S. Although the southern extent of the GFZ is not known precisely, analysis of magnetic anomalies [*Wilson and Hey*, 1995; also D. S. Wilson, personal communication, 2007] and plate motion reconstructions [*Meschede and Barckhausen*, 2000] suggest that the GFZ may have initiated less than 2.6–3.6 My ago, and that its southward termination is likely to the north of 0°S (for a half spreading rate of 25–30 km/My) (Figure 18). Moreover, our results suggest that that the crustal seismic velocity increase observed from west to east is gradual, so it is unlikely to reflect a thermal structure arising from an age offset across a fracture zone. In agreement with plate reconstructions (Figure 18), we suggest that there is no major east-to-west lithospheric age discontinuity beneath the Galápagos platform, and thus we may also rule out this explanation.

[49] The most plausible explanation for the differences in lithospheric strength across the Galápagos platform is that the eastern archipelago was closer to the ridge and the lithosphere was weaker at the time of loading. Models for the deformation of an elastic plate indicate that the flexural rigidity of the lithosphere depends on the thermal age of the lithosphere at the time of loading [*Watts and Zhong*, 2000; *Turcotte and Schubert*, 2002, pp. 331–339]. In support of this interpretation, the gravity anomaly map in Figure 17 shows that the flexural response to loading is present throughout the archipelago, and that this signal is strongest where the age of the lithosphere at the time of loading is oldest. The eastern lithosphere was very young and weak at the time of loading, so its flexural response is less pronounced. In contrast with the specific scenario of *Feighner and Richards* [1994], however, we suggest that the present spatial differences in the strength of the elastic lithospheric may be gradual rather than abrupt.

4.3. Plume-Lithosphere Interactions

[50] As noted earlier, the Galápagos hot spot resembles other oceanic intraplate hot spots in many respects, including its long lifetime, the chemistry of its basalts, its distinctive hot spot trails on two plates, the age progression of associated seamounts, and low seismic velocities in the underlying upper mantle. However, the Galápagos hot spot differs from other hot spots in its broad area of recent volcanic activity, approximately 300 × 200 km^2, and in the east–west differences in lava compositions and volcano morphology, differences thought to be related to volcano location at the time of formation [*Harpp and Geist*, 1998]. We synthesize

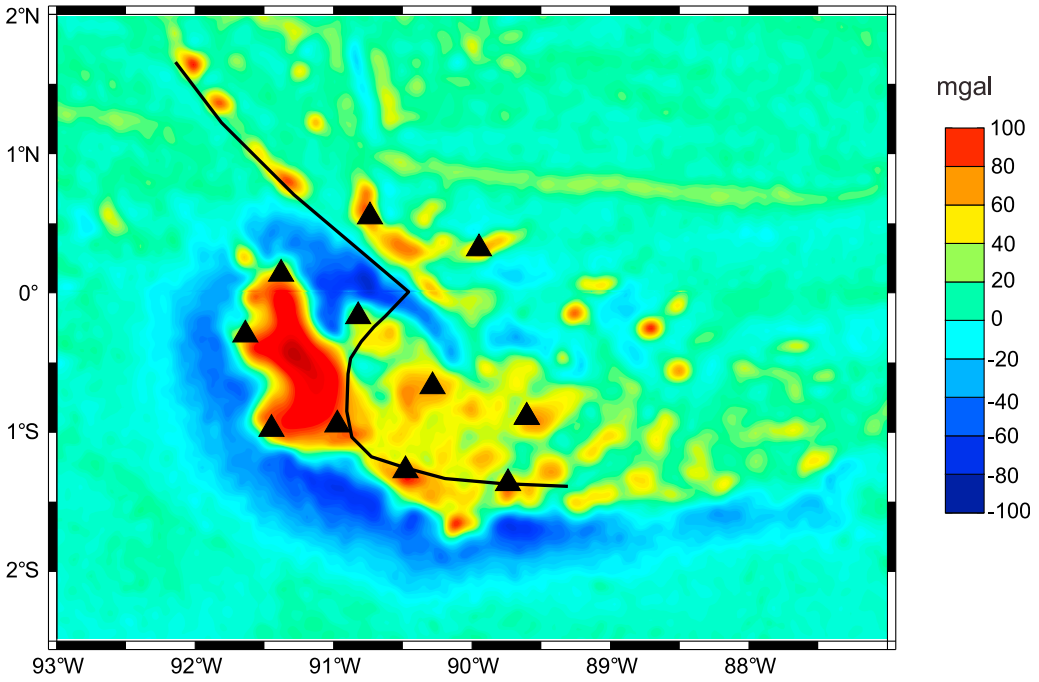

Figure 17. Free air gravity anomaly in the Galápagos region [*Sandwell and Smith*, 1997]. Triangles indicate seismic stations, and the black line shows the locus of the transition from elastically competent lithosphere in the south and west to Airy compensation in the central platform suggested by *Feighner and Richards* [1994].

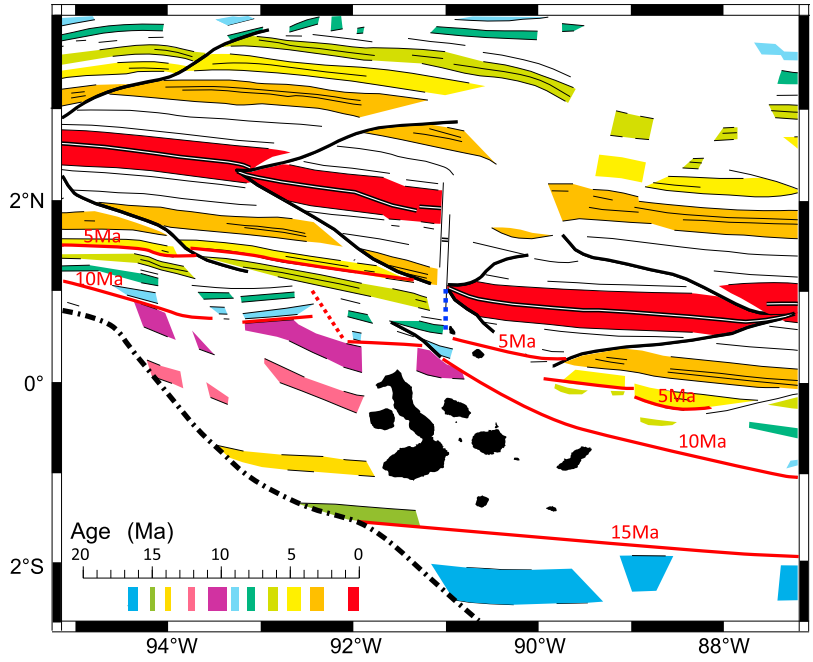

Figure 18. Isochron map of the Galápagos region. Color contours and thin black lines are inferred from magnetic anomalies [*Wilson and Hey*, 1995; *Barckhausen et al.*, 2001; also D. S. Wilson, personal communication, 2007]. Thick black lines show propagator pseudofaults [*Wilson and Hey*, 1995]. The dashed-dotted black line shows the boundary that separates seafloor created at the Galápagos Spreading Center from that formed at the East Pacific Rise [*Barckhausen et al.*, 2001]. Red lines with approximate ages are our interpretation of isochrons from a reconciliation of the magnetic anomalies with paleogeographic reconstructions [*Meschede and Barckhausen*, 2000]. The blue dashed line shows our interpretation of the extent of the Galápagos Fracture Zone (GFZ).

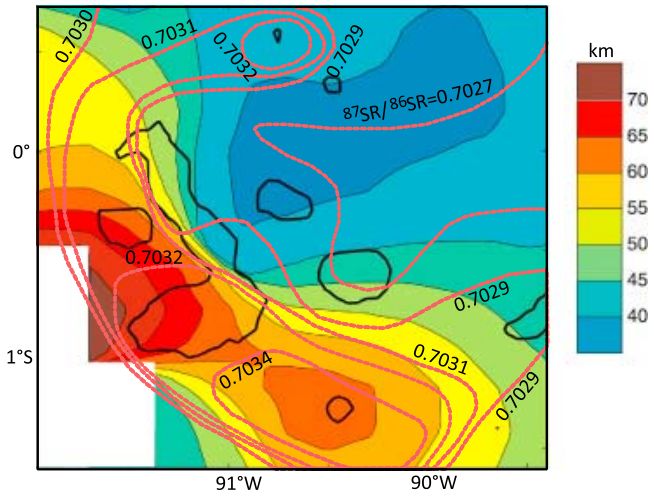

Figure 19. Comparison of estimates of the thickness of the lid of high-mantle seismic velocities (color contours) [*Villagómez et al.*, 2007] with the geographic variation in the $^{87}Sr/^{86}Sr$ ratio of sampled basalts (dashed red lines) [*Harpp and White*, 2001].

our results with earlier work to further elucidate the role of both the mechanical and the chemical lithospheres in controlling spatial variations in magma composition and the alignment of volcanic centers.

[51] A possible explanation for the spatial variability in lava composition is that it reflects unusual dynamics and interaction of the mantle plume with depleted upper mantle [*Geist et al.*, 1988; *Richards and Griffiths*, 1989; *White et al.*, 1993]. By this idea, the current location of the Galápagos plume beneath the western archipelago accounts for the more enriched geochemical signatures of the western volcanoes, whereas mixing of plume material with depleted upper mantle leads to the depleted signatures of the eastern volcanoes. *Geist et al.* [1988], *Richards and Griffiths* [1989], and *White et al.* [1993] proposed that such mixing could be caused by thermal entrainment of depleted mantle into the plume as the upwelling material is sheared eastward by plate drag. Body wave and surface wave tomography [*Toomey et al.*, 2002; *Villagómez et al.*, 2007], however, show no evidence of bending of the plume by plate drag, posing a difficulty for this model at the Galápagos hot spot. In addition, this model predicts that lavas at individual eastern volcanoes should show temporal trends from enriched to more depleted geochemical signatures. However, detailed studies have not revealed age trends in lava composition within single volcanoes [*Geist et al.*, 1998], with the possible exception of Floreana Island in the southern part of the archipelago [*Lyons et al.*, 2007].

[52] A second possibility is that the spatial variability in lava composition is caused by compositional zoning of the plume [*Hoernle et al.*, 2000; *Farnetani et al.*, 2002; *Werner et al.*, 2003]. *Hoernle et al.* [2000] showed that the variability in lava composition occurs at the same relative positions along a geochemical profile across the Galápagos hot spot track off the coast of Costa Rica, suggesting that the spatial zonation of the Galápagos hot spot may be a signature of the source that could have persisted for at least 14 My.

[53] We recently proposed, as an alternative explanation, that variations in the thickness of the thermal and chemical lithosphere contribute to variations in lava composition [*Villagómez et al.*, 2007]. Surface wave tomography has revealed a mantle lid of high seismic velocity and variable thickness beneath the Galápagos region. This lid is interpreted to be higher in viscosity than the underlying convecting mantle because of dehydration during removal of partial melt [*Villagómez et al.*, 2007]. The lid is 60–70 km thick beneath the western and southern part of the archipelago and ~40 km thick beneath the northeastern part (Figure 19). We suggest that the lid to the northeast corresponds to the thermal lithosphere, whereas the bottom of the lid beneath the western and southern parts of the archipelago corresponds to a chemical boundary identified as the base of the residuum from melt removal [*Villagómez et al.*, 2007 Figure 16]. Variations in the thickness of the chemical lithosphere are probably affected by temporal changes in plume-ridge separation and the interaction between the plume and ridge melting zones. The thickness of the seismic velocity lid correlates well with geochemical anomalies (Figure 19). In this scenario, spatial variations in isotopic signatures are due to differences in the amount of melting as a function of depth: enriched lavas to the west and south are consistent with a greater proportion of melting occurring at relatively greater depths, whereas more depleted geochemical signatures result from more extensive partial melting at shallower depths.

[54] Another distinctive characteristic of the Galápagos is that several volcanic centers and seamounts are aligned mostly along northeast and northwest trending lineations (Figure 1), known as the Darwinian lineaments. *Darwin* [1860] first noted that the islands exhibit aligned fractures, and *McBirney and Williams* [1969] showed that the volcanoes themselves are aligned along rectilinear trends. One of the most prominent lineaments is the Wolf-Darwin lineament (WDL) located to the north of the archipelago (Figure 1). Although the origin of these trends is not well known, recent studies suggest that the lineations are controlled by patterns of stress in the lithosphere [*Harpp and Geist*, 2002; *Sinton et al.*, 2003; *Mittelstaedt and Ito*, 2005]. For instance, *Harpp and Geist* [2002] suggested that the WDL is the result of extensional stresses emanating from the inside corner of the transform fault at 91°W. *Sinton et al.* [2003] and *Mittelstaedt and Ito* [2005] suggested that some of the lineations to the north of the archipelago, which appear to radiate from a point near 0° N, 90.7°W [e.g., *Sinton et al.*, 2003, Figure 9], are caused by gravitational stresses resulting from lithospheric uplift by an impinging plume or by the combined effects of the plume and the segmented ridge. However, these explanations do not account for many of the other lineations observed in the western and southern archipelago that do not show a radial pattern, such as the lineations on the J-shaped Isabela Island (Figure 1).

[55] We propose that the northwest and northeast trending Darwinian lineaments that are found throughout the archipelago may be associated with preexisting weaknesses in lithospheric structure that are reactivated by plume-lithosphere interactions. Figure 18 displays a combination of magnetic anomalies [*Wilson and Hey*, 1995; *Barckhausen et al.*, 2001; also D. S. Wilson, personal communication, 2007] and plate reconstructions [*Meschede and Barckhausen*,

2000]. These results show that the Galápagos Spreading Center has undergone a complicated series of ridge jumps and ridge propagation events. Of particular interest is that episodes of ridge propagation result in either V-shaped pseudofaults, where magnetic anomalies are offset, or V-shaped swaths of anomalous crust and lithosphere formed at overlapping spreading centers (OSCs). Beneath the Galápagos Archipelago the trends of the pseudofaults or OSC wakes would be in the northwestern and northeastern directions. Pseudofaults associated with ridge propagation events and wakes of OSCs are likely zones of weakness in the oceanic lithosphere on which the Galápagos Archipelago is constructed. Studies of propagators and OSCs along fast and intermediate spreading ridges indicate that they are tectonically complex and capable of generating discordant zones several tens of kilometers across that are characterized by extensive faulting, block rotation, and crustal alteration [*Carbotte and Macdonald*, 1992; *Canales et al.*, 2003]. Images of crustal-scale normal faults and the distribution of earthquakes within the Juan de Fuca plate system further indicate that propagator wake areas are likely to be more faulted and therefore more hydrated than other parts of the plate system [*Nedimović et al.*, 2009]. We thus infer that most of the northeast and northwest trending Darwinian lineaments may owe their origin to pseudofaults or wakes of OSCs formed during earlier episodes of ridge propagation. By this view, stresses generated by plume-lithosphere interactions reactivated these zones of lithospheric weakness.

5. Conclusions

[56] We have detected lateral variations in the seismic velocity of the crust beneath the Galápagos Archipelago from Rayleigh wave group velocities derived from the cross correlation of records of ambient seismic noise. Our results show that the lowest seismic velocities between 3 and 9 km depth are present beneath the western archipelago, suggesting that the crust in this region is warmer, contains more melt, and is more porous than that beneath the eastern archipelago. The warmer crust lies above the inferred current locus of the Galápagos plume, suggesting that the temperature difference reflects increased magmatic activity and the injection of heat to shallow levels beneath the western archipelago. The west-to-east seismic velocity increase appears to be gradual and correlates well with distance downstream from the hot spot. We propose that the crustal velocity increase is the result of cooling and closing of pore volume.

[57] On the basis of our results, which constrain the broad-scale thermal and chemical structure of the crust and lithosphere, as well as a synthesis of recent plate reconstructions and gravity data, we suggest that both the age of the lithosphere at the time of loading and its thickness and internal structure played major roles in shaping the location of hot spot volcanism and the morphology of volcanic landforms in the Galápagos Archipelago. Variations in the flexural response to loading in the Galápagos, which are correlated with volcano size and morphology, cannot be explained simply by the current thermal state of the lithosphere and more likely reflect varying lithospheric strength at the time of loading. Moreover, spatial variations in isotopic signatures of lavas can be attributed to differences in the amount of melting with depth associated with variations in the thickness of the chemical lithosphere. The thickness of this chemical lithosphere, identified in portions of the region by a high-velocity mantle lid, is probably affected by changes in plume-ridge separation and the interaction between the plume and ridge melting zones. Last, we attribute the northwest and northeast trending Darwinian lineaments that are found throughout the archipelago to preexisting zones of weakness in the lithosphere. Such zones of weakness could have formed as pseudofaults or wakes of OSCs during past episodes of ridge jumps and ridge propagation and then been reactivated more recently by stresses generated by plume-lithosphere interactions.

[58] **Acknowledgments.** We are grateful to Minard Hall of the Instituto Geofísico of the Escuale Politécnica Nacional in Quito, the Charles Darwin Research Station, and the Parque Nacional Galápagos for logistical support and assistance in the field. We also thank two anonymous reviewers for comments that greatly improved this analysis. This research was supported by the National Science Foundation under grants OCE-9908695, OCE-0221549, and EAR-0651123 to the University of Oregon and OCE-0221634 to the Carnegie Institution of Washington.

References

Barckhausen, U., C. R. Ranero, R. von Huene, S. C. Cande, and H. A. Roeser (2001), Revised tectonic boundaries in the Cocos plate off Costa Rica: Implications for the segmentation of the convergent margin and for plate tectonic models, *J. Geophys. Res.*, *106*, 19,207–19,220, doi:10.1029/2001JB000238.

Bensen, G. D., M. H. Ritzwoller, M. P. Barmin, A. L. Levshin, F.-C. Lin, M. P. Moschetti, N. M. Shapiro, and Y. Yang (2007), Processing seismic ambient noise data to obtain reliable broad-band surface wave dispersion measurements, *Geophys. J. Int.*, *169*, 1239–1260, doi:10.1111/j.1365-246X.2007.03374.x.

Canales, J. P., R. S. Detrick, and D. R. Toomey (2003), Segment-scale variations in the crustal structure of 150–300 kyr old fast spreading oceanic crust (East Pacific Rise, 8°15′N–10°5′N) from wide-angle seismic refraction profiles, *Geophys. J. Int.*, *152*, 766–794, doi:10.1046/j.1365-246X.2003.01885.x.

Carbotte, S. M., and K. C. Macdonald (1992), East Pacific Rise 8°–10°30′N: Evolution of ridge segments and discontinuities from SeaMARC II and three-dimensional magnetic studies, *J. Geophys. Res.*, *97*, 6959–6982, doi:10.1029/91JB03065.

Carlson, R. L., and C. N. Herrick (1990), Densities and porosities in the oceanic crust and their variations with depth and age, *J. Geophys. Res.*, *95*, 9153–9170, doi:10.1029/JB095iB06p09153.

Darwin, C. (1860), *The Voyage of the Beagle*, 496 pp., Random House, New York.

Dunn, R. A., V. Lekić, R. S. Detrick, and D. R. Toomey (2005), Three-dimensional seismic structure of the Mid-Atlantic Ridge (35°N): Evidence for focused melt supply and lower crustal dike injection, *J. Geophys. Res.*, *110*, B09101, doi:10.1029/2004JB003473.

Dziewonski, A., S. Bloch, and M. Landisman (1969), A technique for the analysis of transient seismic signals, *Bull. Seismol. Soc. Am.*, *59*, 427–444.

Farnetani, C. G., B. Legras, and P. J. Tackley (2002), Mixing and deformations in mantle plumes, *Earth Planet. Sci. Lett.*, *196*, 1–15, doi:10.1016/S0012-821X(01)00597-0.

Feighner, M. A., and M. A. Richards (1994), Lithospheric structure and compensation mechanisms of the Galápagos Archipelago, *J. Geophys. Res.*, *99*, 6711–6729, doi:10.1029/93JB03360.

Friedrich, A., F. Krüger, and K. Klinge (1998), Ocean-generated microseismic noise located with the Gräfenberg array, *J. Seismol.*, *2*, 47–64, doi:10.1023/A:1009788904007.

Geist, D. J., W. M. White, and A. R. McBirney (1988), Plume-asthenosphere mixing beneath the Galápagos archipelago, *Nature*, *333*, 657–660, doi:10.1038/333657a0.

Geist, D. J., T. R. Naumann, and P. Larson (1998), Evolution of Galápagos magmas: Mantle and crustal fractionation without assimilation, *J. Petrol.*, *39*, 953–971, doi:10.1093/petrology/39.5.953.

Geist, D. J., T. R. Naumann, J. J. Standish, M. D. Kurz, K. S. Harpp, W. M. White, and D. J. Fornari (2005), Wolf Volcano, Galápagos Archipelago: Melting and magmatic evolution at the margins of a mantle plume, *J. Petrol.*, *46*, 2197–2224, doi:10.1093/petrology/egi052.

Grevemeyer, I., and W. Weigel (1997), Increase of seismic velocities in upper oceanic crust: The "superfast" spreading East Pacific Rise at 14°14′S, *Geophys. Res. Lett.*, *24*, 217–220, doi:10.1029/96GL04005.

Gripp, A. E., and R. G. Gordon (2002), Young tracks of hotspots and current plate velocities, *Geophys. J. Int.*, *150*, 321–361, doi:10.1046/j.1365-246X.2002.01627.x.

Harpp, K. S., and D. J. Geist (1998), Galápagos plumology, *Noticias Galápagos*, *59*, 23–28.

Harpp, K. S., and D. J. Geist (2002), Wolf–Darwin lineament and plume–ridge interaction in northern Galápagos, *Geochem. Geophys. Geosyst.*, *3*(11), 8504, doi:10.1029/2002GC000370.

Harpp, K. S., and W. M. White (2001), Tracing a mantle plume: Isotopic and trace element variations of Galápagos seamounts, *Geochem. Geophys. Geosyst.*, *2*, 1042, doi:10.1029/2000GC000137.

Hauff, F., K. Hoernle, H.-U. Schmincke, and R. Werner (1997), A mid Cretaceous origin for the Galápagos hotspot: Volcanological, petrological and geochemical evidence from Costa Rican oceanic crustal segments, *Int. J. Earth Sci.*, *86*, 141–155.

Hey, R. (1977), Tectonic evolution of the Cocos-Nazca spreading center, *Geol. Soc. Am. Bull.*, *88*, 1404–1420, doi:10.1130/0016-7606(1977)88<1404:TEOTCS>2.0.CO;2.

Hoernle, K., R. Werner, J. Phipps Morgan, D. Garbe-Schönberg, J. Bryce, and J. Mrazek (2000), Existence of complex spatial zonation in the Galapagos plume for at least 14 m.y, *Geology*, *28*, 435–438, doi:10.1130/0091-7613(2000)028<0435:EOCSZI>2.3.CO;2.

Hoernle, K., P. van den Bogaard, R. Werner, B. Lissinna, F. Hauff, G. Alvarado, and D. Garbe-Schönberg (2002), Missing history (16–71 Ma) of the Galápagos hotspot: Implications for the tectonic and biological evolution of the Americas, *Geology*, *30*, 795–798, doi:10.1130/0091-7613(2002)030<0795:MHMOTG>2.0.CO;2.

Hooft, E. E. E., D. R. Toomey, and S. C. Solomon (2003), Anomalously thin transition zone beneath the Galápagos hotspot, *Earth Planet. Sci. Lett.*, *216*, 55–64, doi:10.1016/S0012-821X(03)00517-X.

Klein, F. W. (1981), A linear gradient crustal model for south Hawaii, *Bull. Seismol. Soc. Am.*, *71*, 1503–1510.

Larose, E., A. Derode, M. Campillo, and M. Fink (2004), Imaging from one-bit correlations of wideband diffuse wave fields, *J. Appl. Phys.*, *95*, 8393–8399, doi:10.1063/1.1739529.

Lonsdale, P., and K. D. Klitgord (1978), Structure and tectonic history of the eastern Panama Basin, *Geol. Soc. Am. Bull.*, *89*, 981–999, doi:10.1130/0016-7606(1978)89<981:SATHOT>2.0.CO;2.

Lyons, J., D. Geist, K. Harpp, B. Diefenbach, P. Olin, and J. Vervoort (2007), Crustal growth by magmatic overplating in the Galápagos, *Geology*, *35*, 511–514, doi:10.1130/G23044A.1.

Malcolm, A. E., J. A. Scales, and B. A. van Tiggelen (2004), Extracting the Green function from diffuse, equipartitioned waves, *Phys. Rev.*, *70*, 015601.

McBirney, A. R., and H. Williams (1969), Geology and petrology of the Galápagos Islands, *Mem. Geol. Soc. Am.*, *118*, 197 pp.

Meschede, M., and U. Barckhausen (2000), Plate tectonic evolution of the Cocos-Nazca spreading center, in *Proceedings of the Ocean Drilling Program, Scientific Results*, vol. 170, edited by E. A. Silver et al., pp. 1–10, Ocean Drilling Program, College Station, Tex.

Metropolis, N., and S. Ulam (1949), The Monte Carlo method, *J. Am. Stat. Assoc.*, *44*, 335–341, doi:10.2307/2280232.

Mittelstaedt, E., and G. Ito (2005), Plume-ridge interaction, lithospheric stresses, and the origin of near-ridge volcanic lineaments, *Geochem. Geophys. Geosyst.*, *6*, Q06002, doi:10.1029/2004GC000860.

Morgan, W. J. (1972), Deep mantle convection plumes and plate motions, *Am. Assoc. Pet. Geol. Bull.*, *56*, 617–618.

Mosegaard, K., and A. Tarantola (1995), Monte Carlo sampling of solutions to inverse problems, *J. Geophys. Res.*, *100*, 12,431–12,447, doi:10.1029/94JB03097.

Nedimović, M. R., D. R. Bohnenstiehl, S. M. Carbotte, J. P. Canales, and R. P. Dziak (2009), Faulting and hydration of the Juan de Fuca plate system, *Earth Planet. Sci. Lett.*, *284*, 94–102, doi:10.1016/j.epsl.2009.04.013.

Richards, M. A., and R. M. Griffiths (1989), Thermal entrainment by deflected mantle plumes, *Nature*, *342*, 900–902, doi:10.1038/342900a0.

Ritzwoller, M. H., N. M. Shapiro, M. P. Barmin, and A. L. Levshin (2002), Global surface wave diffraction tomography, *J. Geophys. Res.*, *107*(B12), 2335, doi:10.1029/2002JB001777.

Sabra, K. G., P. Gerstoft, P. Roux, W. A. Kuperman, and M. C. Fehler (2005), Extracting time-domain Green's function estimates from ambient seismic noise, *Geophys. Res. Lett.*, *32*, L03310, doi:10.1029/2004GL021862.

Saito, M. (1988), DISPER80: A subroutine package for calculation of seismic normal-mode solutions, in *Seismological Algorithms: Computational Methods and Computer Programs*, edited by D. J. Doornbos, pp. 293–319, Academic, San Diego, Calif.

Sallarès, V., P. Charvis, E. R. Flueh, and J. Bialas, and the SALIERI Scientific Party (2005), Seismic structure of the Carnegie Ridge and the nature of the Galápagos hotspot, *Geophys. J. Int.*, *161*, 763–788, doi:10.1111/j.1365-246X.2005.02592.x.

Sandwell, D. T., and W. H. F. Smith (1997), Marine gravity from Geosat and ERS 1 satellite altimetry, *J. Geophys. Res.*, *102*, 10,039–10,054, doi:10.1029/96JB03223.

Shapiro, N. M., and M. Campillo (2004), Emergence of broadband Rayleigh waves from correlations of the ambient seismic noise, *Geophys. Res. Lett.*, *31*, L07614, doi:10.1029/2004GL019491.

Shapiro, N. M., M. Campillo, L. Stehly, and M. Ritzwoller (2005), High-resolution surface wave tomography from ambient seismic noise, *Science*, *307*, 1615–1618, doi:10.1126/science.1108339.

Shaw, P. R. (1994), Age variations of oceanic crust Poisson's ratio: Inversion and a porosity evolution model, *J. Geophys. Res.*, *99*, 3057–3066, doi:10.1029/93JB02109.

Sinton, C. W., D. M. Christie, and R. A. Duncan (1996), Geochronology of Galápagos seamounts, *J. Geophys. Res.*, *101*, 13,689–13,700, doi:10.1029/96JB00642.

Sinton, J., R. Detrick, J. P. Canales, G. Ito, and M. Behn (2003), Morphology and segmentation of the western Galápagos Spreading Center, 90.5°–98°W: Plume-ridge interaction at an intermediate spreading ridge, *Geochem. Geophys. Geosyst.*, *4*(12), 8515, doi:10.1029/2003GC000609.

Spudich, P., and J. Orcutt (1980), A new look at the seismic velocity structure of the oceanic crust, *Rev. Geophys.*, *18*, 627–645, doi:10.1029/RG018i003p00627.

Tarantola, A., and B. Valette (1982), Generalized nonlinear inverse problems solved using the least squares criterion, *Rev. Geophys.*, *20*, 219–232, doi:10.1029/RG020i002p00219.

Ten Brink, U. S., and T. M. Brocher (1987), Multichannel seismic evidence for a subcrustal intrusive complex under Oahu and a model for Hawaiian volcanism, *J. Geophys. Res.92* 13,687–13,707, doi:10.1029/JB092iB13p13687.

Tikhonov, A. N. (1943), On the stability of inverse problems, *Dokl. Akad. Nauk SSSR*, *39*(5), 195–198.

Toomey, D. R., E. E. E. Hooft, and R. S. Detrick (2001), Crustal thickness variations and internal structure of the Galápagos Archipelago, *Eos Trans. AGU*, *82*(47), Fall Meet. Suppl., Abstract T42B–0939.

Toomey, D. R., E. E. E. Hooft, S. C. Solomon, D. E. James, and M. L. Hall (2002), Seismic evidence for a plume beneath the Galápagos hotspot, *Eos Trans. AGU*, *83*(47), Fall Meet. Suppl., Abstract S72C–02.

Turcotte, D. L., and G. Schubert (2002), *Geodynamics*, 2nd ed., 456 pp., Cambridge Univ. Press, New York.

Vera, E. E., J. C. Mutter, P. Buhl, J. A. Orcutt, A. J. Harding, M. E. Kappus, R. S. Detrick, and T. M. Brocher (1990), The structure of 0− to 0.2 −m.y.-old oceanic crust at 9°N on the East Pacific Rise from expanded spread profiles, *J. Geophys. Res.*, *95*, 15,529–15,556, doi:10.1029/JB095iB10p15529.

Villagómez, D. R., D. R. Toomey, E. E. E. Hooft, and S. C. Solomon (2007), Upper mantle structure beneath the Galápagos Archipelago from surface wave tomography, *J. Geophys. Res.*, *112*, B07303, doi:10.1029/2006JB004672.

Watts, A. B., and S. Zhong (2000), Observations of flexure and the rheology of oceanic lithosphere, *Geophys. J. Int.*, *142*, 855–875, doi:10.1046/j.1365-246x.2000.00189.x.

Werner, R., K. Hoernle, P. van der Bogaard, C. Ranero, R. von Huene, and D. Korich (1999), Drowned 14−m.y.-old Galápagos archipelago off the coast of Costa Rica: Implications for tectonic and evolutionary models, *Geology*, *27*, 499–502, doi:10.1130/0091-7613(1999)027<0499:DMYOGP>2.3.CO;2.

Werner, R., K. Hoernle, U. Barkckhausen, and F. Hauff (2003), Geodynamic evolution of the Galápagos hot spot system (Central East Pacific) over the past 20 m.y.: Constraints from morphology, geochemistry, and magnetic anomalies, *Geochem. Geophys. Geosyst.*, *4*(12), 1108, doi:10.1029/2003GC000576.

White, W. M., A. R. McBirney, and R. A. Duncan (1993), Petrology and geochemistry of the Galápagos Islands: Portrait of a pathological mantle plume, *J. Geophys. Res.*, *98*, 19,533–19,563, doi:10.1029/93JB02018.

Wilcock, W. S. D., S. C. Solomon, G. M. Purdy, and D. R. Toomey (1995), Seismic attenuation structure of the East Pacific Rise near 9°30′N, *J. Geophys. Res.*, *100*, 24,147–24,166, doi:10.1029/95JB02280.

Wilson, D. S., and R. N. Hey (1995), History of rift propagation and magnetization intensity for the Cocos-Nazca spreading center, *J. Geophys. Res.*, *100*, 10,041–10,056, doi:10.1029/95JB00762.

Zhou, Y., F. A. Dahlen, and G. Nolet (2004), Three-dimensional sensitivity kernels for surface wave observables, *Geophys. J. Int.*, *158*, 142–168, doi:10.1111/j.1365-246X.2004.02324.x.

E. E. E. Hooft, D. R. Toomey, and D. R. Villagómez, Department of Geological Sciences, University of Oregon, Eugene, OR 97403, USA. (darwin7@gmail.com)

S. C. Solomon, Department of Terrestrial Magnetism, Carnegie Institution of Washington, Washington, DC 20015, USA.